Dynamic modulation of fimbrial extension and FimH-mannose binding force on live bacteria under pH changes: a molecular atomic force microscopy analysis.

A Jacquot, C Sakamoto, Angelina Razafitianamaharavo, C Caillet, J Merlin, A Fahs, G Ghigo, C Beloin, J F L Duval, G Francius

Dynamic modulation of fimbrial extension and FimH-Mannose binding force on live bacteria under pH changes: a molecular AFM analysis

Jacquot A.[1,2], Sakamoto C.[5,6], Razafitianamaharavo. A[3,4], Caillet C.[2,3], Merlin J.[2,3], Fahs A.[1,2], Ghigo J.M.[5], Beloin C.[5#], Duval J.F.L.[3,4#] and Francius G.[1,2*]

[1] Université de Lorraine, Laboratoire de Chimie Physique et Microbiologie pour l'Environnement, UMR 7564, Villers-lès-Nancy, F-54601, France.

[2] CNRS, Laboratoire de Chimie Physique et Microbiologie pour l'Environnement, UMR 7564, Villers-lès-Nancy, F-54601, France.

[3] Université de Lorraine, Laboratoire Interdisciplinaire des Environnements Continentaux, UMR 7360, 15 avenue du Charmois, Vandoeuvre-lès-Nancy, F-54501, France.

[4] CNRS, Interdisciplinaire des Environnements Continentaux, UMR 7360, 15 avenue du Charmois, Vandoeuvre-lès-Nancy, F-54501, France.

[5] Institut Pasteur, Unité de Génétique des Biofilms, 25-28 rue du Dr Roux, Paris cedex 15, F-75724, France.

[6] Université Paris Diderot, Sorbonne Paris Cité, Paris, F-75205, France.

Keywords:

Single molecule force spectroscopy, type 1 fimbriae, unwinding, AFM, bacteria

[#]: equivalent contribution

* Corresponding author:

Email: gregory.francius@univ-lorraine.fr

Phone: (33) 03 83 68 52 36

Abstract

Mechanical and conformational properties of type 1 fimbriae were evaluated on live bacterial cells by Single Molecule Force Spectroscopy (SMFS) and Dynamic Force Spectroscopy (DFS) in buffered solutions whose pH varied from 3 to 9. We evidenced that both fimbrial extension and fimbrial binding force to mannosylated-surface are modulated with changing the externally applied shear force and the solution pH. In particular, intertwined FimA-FimA and FimH-mannose interactions lead to a 5 to 25-fold decrease of the fimbrial unwinding for pulling rates larger than 10 μm/s and for pH values outside the range 5 to 7. In this pH range, the FimH-mannose binding force is maximal with a magnitude of ~150-200 pN and the fimbriae extension reaches 8 μm. The enhancement of the FimH-mannose binding force at neutral pH, as evidenced from molecular AFM analyses, strongly correlates with an optimum in yeast agglutination detected at pH 5 to 7. The results reported in this work suggest that "catch bond effect" was negligible over the range of pulling rates tested, and both FimA-FimA and FimH-mannose interactions under given pH and external shear force conditions modify the ability of the bacteria to efficiently colonize host surfaces.

Introduction

Early adhesion events with environmental surfaces or host tissues and subsequent interactions between bacteria initiate biofilm formation and are considered, in the case of pathogenic bacteria, as key steps of colonization/infection processes. Therefore, the investigation of molecular factors together with the mechanisms governing these early adhesion events has emerged as a critical point to understand the infection process and consequently to potentially develop alternative strategies to antibiotics in order to prevent bacterial adhesion to surfaces.

The adhesive bonds between bacteria and surfaces or between bacteria are subjected to tensile mechanical forces that possibly depend on parameters such as solution pH, osmolarity or temperature. A successful surface colonization reflects the ability of the bacteria to withstand natural detachment forces and environmental perturbations once anchored at the target surface. A relevant example of successful colonizers of human mucosa is *E. coli*. These bacteria are natural inhabitants of the gastro-intestinal tract and they may behave both as commensal and pathogenic entities. As pathogens, they can be at the origin of intra-intestinal diseases like diarrhea caused by enterohaemmoragic or enteroaggregative *E. coli* (EHEC and EAEC respectively), or extra-intestinal diseases, *e.g.* urinary tract infections caused by uropathogenic *E. coli* (UPEC). In the gastro-intestinal and urinary tracts, *E. coli* is exposed to shear forces imposed by mechanical host defenses (mucus and urine flows) and to changes in pH. This suggests that the mechanical and chemical properties of *E. coli* cell wall are key factors that make it possible for the bacteria to sustain competing shear forces and drastic changes in environmental conditions and thereby to colonize efficiently specific hosts' sites.

Bacterial adhesion is mainly mediated by specific non-covalent bonds between tethered ligands and receptors.[1] The adhesion further generally involves proteinaceous molecules or macromolecular complexes referred to as adhesins, *i.e.* monomeric or polymeric polymers forming fimbrial or afimbrial structures brought to the bacterial surface by various secretion

systems.[2, 3] In *E. coli*, the two major classes of adhesins are (i) fimbrial adhesins transported by the chaperone-usher pathway, and (ii) afimbrial adhesins transported by type V secretion pathway. Prototypical chaperone-usher fimbriae of *E. coli* are P pili and type 1 fimbriae, which are commonly associated to UPEC and infections in the upper and the lower urinary tract, respectively.[4] The structure of these hairy surface appendages are very similar, but differ in terms of biomechanical properties.[5] Type 1 fimbriae are rod-shaped filaments consisting of FimA repeating subunits terminated by a specific adhesin called FimH that binds to α-D-mannosylated proteins, [6, 7] while P pili consist of PapA subunits terminated by the PapG adhesin whose variants bind to different glycolipids.[8, 9]

Since the last decade, atomic force microscopy (AFM) has emerged as a powerful tool for probing microbial surfaces and interfacial phenomena, in particular specific and non-specific interactions at the nanoscale.[10-13] Dynamic Force Spectroscopy (DFS) and Single-Molecule Force Spectroscopy (SMFS) are derivative AFM techniques that provide access to molecular dynamic processes, chemical or surface reactivity, macromolecular conformational features, and interactions between single molecules.[14, 15] Recent mechanical measurements were performed on P pili and type 1 fimbriae using Force Measuring Optical Tweezers (FMOT). It was reported that both pili are highly flexible and they may be viewed as dynamic structures with spring-like properties.[5, 16-18] Indeed, when bacteria were subjected to hydrodynamic constrains, these structures maintain bacterial attachment to host cells or surfaces by reducing the impact of flushes and associated mechanical stress [5, 19] following an unwinding of the pilus rod's helical quaternary structure anchored at the colonized surface. Several studies pointed out that the length of P-pili and type 1 fimbriae could increase by a factor 5 following such unwinding process under high shear stress conditions.[20-22] The forced unraveling of type 1 fimbriae is reversible, with helical rewinding taking place for shear forces of magnitude ~ 60 pN.[17, 23] Although the dynamic elongation properties of pili have been investigated by

AFM, optical tweezers or DFS, no studies has focused so far on the role of environmental factors like external pH.

In view of the various pH exposure conditions possibly encountered by *E. coli* in its natural environment, we report here a systematic investigation of the impact of pH on the dynamic elongation of type 1 fimbriae and on the adhesion force between such structures and sugar-coated surfaces. For that purpose, AFM-tips were functionalized with mannose to probe the specific interactions with FimH, the lectin ending part of fimbrial rods. We recorded retraction SMFS force curves at different pH values in the range 3.2 to 9.2. Data were analyzed on the basis of Worm Like Chain (WLC) model in order to quantify the impact of pH on the conformational properties of type 1 fimbriae. In addition, dynamic force spectroscopy (DFS) measurements were performed to analyze the elongation of type 1 fimbriae under various pH conditions over a large range of tip retraction speeds, thus exploring the effect of adverse shear force experienced by cells when attached to target surfaces. DFS and SMFS experiments were further correlated to macroscopic type 1 fimbriae-dependent yeast agglutination assays with *E. coli*. Overall, the study highlights that fimbrial unwinding strongly depends on pH and is mediated by the corresponding modulation of the FimA-FimA interactions all along the fimbriae structure. In addition, the molecular interactions between FimH and mannose are significantly impacted both by retraction speed and solution pH. This in turn could probably modify the ability of the bacteria to efficiently colonize host surfaces.

Materials and Methods

Bacterial strains.

The *E. coli* K-12 strains used in this study are listed and described in previous works.[24, 25] These isogenic strains were constructed from *Escherichia coli* MG1655 (*E. coli* genetic stock

center CGSC#6300). All strains used in this study contain the *gfpmut3* gene linked to the *bla* ampicillin resistance gene (*amp*^{R}, 100 µg/mL) that makes them fluorescent, and a deletion of the *fliE* to *fliR* genes replaced by the *cat* chloramphenicol resistance gene (*cm*^{R}, 25 µg/mL). Our reference strain (E2152) has been additionally deleted for both the *fim* operon encoding type 1 fimbriae (Δ*fimA-H*::*zeo, zeo*^{R} 50 µg/mL) and *agn43* gene (Δ*flu*::*km*, *km*^{R} 100 µg/mL). The constitutive production of type 1 fimbriae was ensured by insertion of a constitutive promoter in front of the *fim* operon (strain with PcL*fim*, E2146).[25-27]

Growth conditions and sample preparation for AFM experiments.

Bacteria were pre-grown overnight at 37°C under agitation (150 rpm) in M63B1 minimal medium supplemented with 0.4% glucose (M63B1glu) and with the appropriate antibiotics for the proper selection of the strain of interest. The next day, fresh M63B1glu medium was inoculated with the overnight culture to an OD_{600} of *c.a.* 0.05 and cultivated under the same conditions until the biomass reached an OD_{600} of 0.5-0.6.

Then, 2 mL of the bacterial suspension were removed and placed on a PEI-silicon wafer slide for 30 minutes. The samples were extensively rinsed with PBS solution to remove M63B1glu and placed directly into the AFM closed fluid-cell with 2 mL of PBS solution at the desired pH in the range 3 to 9.

Electrophoretic mobility measurements.

We performed electrophoretic mobility (EPM) measurements on bacteria in a quartz suprasil cell at 24°C (Zetaphoremeter IV, CAD Instrumentations, Les Essarts le Roi, France). Displacements of bacterial cells were followed from the reflection by bacteria of a laser beam tracked with a charge-coupled device camera. Using image analysis software, recorded images were processed in real time to calculate the electrophoretic mobilities from the migration motion of bacteria subjected to a constant direct-current electric field (800V/m). Different cycles were recorded to carry out 100 measurements of bacterial mobility in M63B1

minimal medium supplemented with 0.4% glucose (M63B1glu). Additionally, the reproducibility of the experiments was addressed by repeating the electrokinetic measurements with at least three different freshly-prepared bacterial suspensions.

Measurement of *E. coli* type 1 fimbriae-mediated yeast agglutination.

We assessed the capacity of type 1 fimbriae to agglutinate yeast cells following a protocol previously described.[28] Briefly, 5 mL of bacteria and yeast cultures grown to stationary phase in LB or YPD (Yeast extract Peptone-Dextrose) respectively, were diluted to reach an optical density at 600 nm (OD_{600nm}) of 1.0. Bacteria and yeast cells were washed with phosphate saline buffer (PBS) 1X and resuspended in PBS1X with pH 3 to 9. Bacteria were then mixed with yeast (OD_{600nm} 1:1) and placed in a 96-well microtiter plate and agglutination was then assessed after 10 min settling. Agglutination titers were expressed as the lowest bacterial concentration leading to yeast agglutination.

Chemicals and AFM-tips functionalization.

Mannosamine ($C_6H_{11}O_5$-NH_2), ethanolamine (C_2H_7NO), dimethylsulfoxyde (DMSO), triethylamine ($C_6H_{15}N$), sodium cyanoborohydride ($NaCNBH_3$) and PBS tabs were purchased from Sigma-Aldrich (Sigma Aldrich, Saint-Quentin Fallavier, France) and used as received. PEG-acetal linkers were purchased from Hermann Gruber group (Institute of Biophysics, University of Linz, Austria).

AFM-tips were functionalized with mannosamine using a procedure previously described[12, 29] for the detection and stretching of type 1 fimbriae. Briefly, silicon nitride tips (MLCT, Bruker Nano AXS, Palaiseau, France) were first modified with amino groups that further reacted with PEG linkers carrying benzaldehyde functions. The latter were then directly attached to mannosamine through terminal NH_2 group.

AFM imaging, Single-Molecule Force Spectroscopy (SMFS) and Dynamic Force Spectroscopy (DFS) measurements.

AFM images were recorded with FastScan AFM (Bruker AXS, Palaiseau, France) and force-distance curves with a MFP3D-BIO instrument (Asylum Research Technology, Atomic Force F&E GmbH, Mannheim, Germany). Silicon nitride and gold coated cantilevers of conical shape were purchased from Bruker (MLCT and NPG, Bruker AXS, Palaiseau, France) with spring constants of 10-12 pN/nm and 120-150 pN, respectively. Experiments were performed in PBS at different pH values from 3 to 9 and at room temperature.

Adhesion forces, conformational characteristics and extension of the adhesins were measured by recording Force-Volume Images (FVI) consisting of a grid of 32-by-32 force curves obtained upon approach and subsequent retraction of the tip (SMFS experiments) and for pulling rates of magnitude 0.5-20 µm/s (DFS experiments). Force measurements were performed in triplicate for each condition examined over an area of 5 µm × 5 µm after locating single bacteria *via* the Olympus IX 71 inverted microscope that supports the AFM. Biological replicates from independent bacterial growth culture, and performed at pH 7 for the 6 pulling rates were close to the triplicates with less than 10% deviation (data not shown). The uncertainties given in this work were calculated from the technical triplicates only.

In SMFS experiments, the adhesins located on the gold-surfaces and on the biological samples are stretched upon removal of the chemically-modified AFM tip away from the surface (Figure S1 in Supporting Information). The obtained force *versus* distance curves are then analyzed using WLC (Worm Like Chain) model. This model is most suitable and most frequently used to describe the extension of polypeptides. Within the framework of this theory, the extension z of the macromolecule is related to the retraction force F_{adh} *via*

$$F_{\mathrm{adh}}(z) = -\frac{k_B T}{l_p}\left[\frac{z}{L_c} + 4\left(1-\frac{z}{L_c}\right)^{-2} - \frac{1}{4}\right] \qquad (1)$$

where the persistence length l_p directly reflects the chain stiffness, L_c is the total contour length of the macromolecule and k_B is the Boltzmann constant.

The number of monomers in the polypeptidic chains is provided by

$$N = \frac{L_c}{l_p} \tag{2}$$

All the FVI were automatically analyzed with a Matlab algorithm described elsewhere.[24] It is emphasized that force-distance curves measurements were performed on freshly prepared PEI-coated glass slice and Concanavalin A-grafted gold surface in order to (successfully) verify the binding specifity of the AFM tip.

Results and discussion

Morphological analysis of cells constitutively expressing type 1 fimbriae.

To gain insight into the cell surface morphology of *E. coli* K-12 producing type-1 fimbriae, live bacterial cells were grown at 37°C and electrostatically immobilized onto a PEI-coated silicone substrate and gently dehydrated before imaging by AFM (Figure 1). The AFM images clearly showed that the cells constitutively expressing type 1 fimbriae (E2146) exhibited a 2 to 2.5 µm rod-like shape decorated with 10 nm diameter filamentous surface structures of length 50 to 500 nm. These characteristics well correspond to those reported for type 1 fimbriae, *i.e.* rod-shaped and helical structure of total contour length 1 to 10 µm and diameter 6 to 20 nm.[30, 31] Adhesion images also evidenced a pronounced disparity in terms of length of the surface appendages as some are partially retracted and others are completely collapsed along the contour of the cell wall. These observations underpin some flexibility of type 1 fimbriae structures, probably depending on their physiological state, in line with previous conclusions.[5, 16-18]

Impact of pH and pulling rate on FimH-mannose interaction.

We performed single-molecule and dynamic force spectroscopy measurements (SMFS and DFS) on type 1 fimbriae anchored at the wall of living cells using mannose functionalized cantilevers (Figure S1) in order to (i) quantify the adhesion force between type 1 fimbriae and AFM-tip functionalized with mannosyl residues, (ii) estimate the impact of pH on the conformational properties of the type 1 fimbriae structure as derived from analysis of the retraction force curves using eq 1 described in the Materials and Methods section, and (iii) investigate the dynamic behaviour of type 1 fimbriae submitted to increasing pulling rates, which somehow mimics the effect of external shear forces the cells experience when attached to host-tissue surfaces. Indeed, previous study evidence that between the bladder and the kidney, urine flow can reach up to 30,000 μm/s.[32]

Typical force curves and corresponding statistic distribution of the adhesion forces obtained at pH 7.4 for pulling rates of 2 and 20 μm/s are reported in Figure 2. A typical elongation force-curve of type 1 fimbriae is generally composed of three distinct regimes as reported in literature.[17, 33] In the first regime, the force increases in absolute value upon retraction of the AFM tip, which corresponds to the stretching of the fimbriae structure until a force plateau is reached. This plateau is symptomatic of a tensed helical structure where the FimA units that predominantly constitute the fimbrial filament retain their conformation. In the second regime, the interactions between successive FimA units are broken at constant force, *i.e*. the fimbrial filament is unfolded and there is unwinding of the FimA units constituting the fimbrial rod. In a last regime the force gradually increases (in absolute value) and abruptly decreases to zero. This drop is related to the rupture between the FimH lectin-ending part of the fimbrial structure and mannose grafted on the tip. Regardless the value of the retraction speed of the AFM tip, we systematically measured for the last detected adhesion event a force plateau of about 62 ± 11 pN. The occurrence of single and multiple adhesive events per force curve reflects the simultaneous detection, unfolding and rupture of one or several fimbriae

captured by the tip. We underlined that the contact depth between the cell wall surface and the functionalized AFM-tip was fixed to 20 nm, which avoids the attachment of too many fimbriae on the probe's apex.

For both pulling rates aforementioned, we found similar retraction force curves characterized by the three characteristic regimes discussed above. However, different multimodal distributions for the rupture force (or FimH-mannose bond rupture force) can be identified (Tables 1 and 2). In details, the first adhesion force in this distribution (Figures 2c, 2d) significantly decreases from 95 ± 25 to 70 ± 19 pN while increasing the pulling rate by a factor 10, and the second rupture force value decreases from 169 ± 21 to 141 ± 43 pN for similar changes in pulling rates. This 16% to 26% decrease in rupture force may be related to the decrease of the interaction time between the FimH lectin domain and the mannosyl residue grafted on the AFM-tip upon increase of the pulling rate.

Furthermore, close inspection of Figure 2 reveals two concomitant phenomena when the pulling rate is increased by a factor 10. First, the largest rupture force detected in the multimodal distribution increases from 244 pN up to 281 pN with increasing the pulling rate, while the last rupture distance decreases from about 3.5 μm to 2 μm (see next section for discussion of this feature).

The qualitative dependence of the first two rupture forces on pulling rate is not in agreement with the so-called "catch bond effect" reported in the literature [23, 34] for FimH adhesins. According to such an effect, the adhesion of FimH onto glucose-coated surfaces is favored with increasing flow rates or, equivalently, as the adhesive bonds are strengthened by tensile mechanical forces. In this study, AFM measurements were carried out with pulling rates that are 10 to 100 times larger than those in line with a "catch bond effect". We therefore believe that our experiments are probably performed outside the range of pulling rate magnitude that leads to increased adhesion with increasing pulling force. Despite these discrepancies, the

adhesion forces corresponding to the interaction between AFM tip and a given fimbriae as measured here are comparable in magnitude to those reported in literature.[33] These results indicate that the mechanical response of type 1 fimbriae may depend on flow rates according to processes that are different than those leading to the catch bond effect. In particular, Figure 2 suggests that the strength of FimH-mannose adhesion depends on the interplay between the characteristic time scales pertaining to FimH-mannose interaction and to the retraction dynamics of the mannose residues from the FimH ending units. In the next section, we further discuss the dependence of the last rupture distance on pulling rate.

Modeling the experimental stretching of type 1 fimbriae using worm-like-chain model.

The retraction force curves depicted in Figures 2a, 2b were interpreted using the Worm like Chain (WLC) model (eq 1). Following this strategy, we derived two key-parameters pertaining to the structural properties of the type 1 fimbriae:

- the contour length L_c defined as the length of the fully extended linear polypeptidic chain.
- the persistence length l_p that reflects the intrinsic flexibility or rigidity of the polypeptidic chain.

A careful analysis of these L_c and l_p parameters enables to identify the structural or conformational changes of the fimbriae-mannose chain during its extension. The statistic distribution of l_p and L_c values obtained at pH 7.4 with 2 and 20 µm/s pulling rates are reported in Figure 3. For both conditions of pulling rate tested in this work, similar bimodal distributions of L_p are found with values 0.05 ± 0.03 nm and 0.21 ± 0.07 nm (Tables 1 and 2), which is in close agreement with data derived from WLC modeling of complex proteins like myosin [35]. The lowest l_p value further matches the typical pitch distance for a β-helix while the second value adequately compares to the typical pitch distance for an α-helix [36, 37] or α-

helix rise per amino acids.[38-40] This result is in good agreement with conformation of the fimbrial subunits that are characterized by β-sheet for FimH (Ig-like domains) whereas the stacking of FimA leads to formation of α-helix structure. Altogether, the above results indicate that the obtained persistence length that reflects the very flexibility of the FimH adhesin, is not affected with increasing pulling rates at fixed solution pH. This conclusion is further supported by the systematic analysis of force-separation distance curves recorded at a fixed pH value in the range 3 to 9 and different pulling rates 2, 5, 10 and 20 μm/s (Figure S2 in Supporting Information).

The distribution in total contour length L_c at pH 7.4 is broad (Figure 3c), starting from 0.2 μm up to 10 μm at a pulling rate of 2 μm/s. When the pulling rate is increased to 20 μm/s (Figure 3d), a narrower distribution is found with L_c values in the range 0.2 μm to 2 μm and a weak distribution in the range of 2 μm to 6 μm, which is in line with literature.[41] In order to further rationalize this dependence of L_c on pulling rate as derived from force curve modeling, we report in Figure 4 the pH- and pulling rate-mediated variations of the maximal elongation of type 1 fimbriae prior to the last rupture event detected in the force curves. The reader is referred to Figure S3 for typical force curves data collected at various pH values and 2 μm/s pulling rate, and to Figure S4 for corresponding statistical distribution in maximal elongation length (Table S1). For pulling rates of 0.5 to 20 μm/s, the maximal extension of the fimbriae obviously depends on solution pH (Figure 4). In details, the maximal extension increases with increasing pH and reaches a pronounced maximum at pH 7.4 (pH of PBS buffer with no addition of acid or base) before decreasing to values lower than 0.5 μm with further increasing pH. The largest value of the maximum extension amplitude is ~8 μm for pulling rates lower than 5 μm/s and it gradually decreases to 3 μm with increasing pulling rate from 5 to 20 μm/s. Overall, the results displayed in Figure 4 suggest that the interactions between the FimA units in the fimbrial rod are strongly affected by changes in solution pH and in pulling

rate. In particular, the collapse of the fimbrial structure length with increasing pulling rate is likely related to the marked dynamic nature of the FimA-FimA units interactions within the fimbrial rod, as detailed in Puorger *et al.*[42] This dependence of the FimA-FimA units interactions on pulling rate also results in a decrease of the last rupture force at fixed pH value, as shown in Figures 2c and 2d.

The understanding of the above features pertaining to the maximal elongation of the fimbrial structure (Figure 4) deserves additional comments. Several studies have evidenced that a decrease in rupture force with increasing pulling rate is related to changes in dynamics of fimbrial unwinding. These changes are governed by weak layer-to-layer interactions (of *e.g.* hydrophobic nature) between subunits on adjacent helical structures, and by the nearly horizontal orientation of Fim protein subunits (FimA, FimG and FimF) with respect to the filament axis.[21, 22, 43] The dependence of CFA/I (colonization factor antigen I) pili rupture force on pulling rate was observed for pulling rate larger than a critical value (1.4 μm/s) referred to as the corner velocity.[21] Our results are consistent with pulling rate dependent-rupture force and elongation as reported for CFA/P/I pili [19, 22, 44], and they additionally evidence a strong influence of solution pH on the extent of fimbrial unwinding, as schematically illustrated in Figure S5 and Figure S6.

The impact of pH and medium salinity on the elongation of pili was previously reported for P pili [43] without solid mechanistic explanation for the observed trends, and such data are not available for type 1 pili. We believe that fimbrial unwinding becomes incomplete for pulling rates larger than the corner velocity because retraction dynamics is too fast to allow a sufficient time delay to undo the connections (hydrogen bonds, salt bridges and hydrophobic contacts) between FimA units.[45-47] It is also expected that a decrease of the solution pH leads to stronger hydrogen bonds inside the fimbrial rod therefore reducing the fimbrial unwinding. This reduction in elongation is also observed under alkaline conditions where negative

charges issued from deprotonated carboxylic groups likely increase the degree of connectivity between FimA units, which *in fine* results in decreased unwinding amplitude.

Dependence of FimH-mannose binding force on pulling rate and pH

In Figure 5, the modulations of the average FimH-mannose rupture force is displayed as a function of solution pH for various values of pulling rate: 0.5, 1, 2, 5, 10 and 20 µm/s. It is recalled that the last rupture force corresponds to the strength of the FimH-mannose bond. For the lowest pulling rate tested, the adhesion force basically remains independent of pH and equals 60-80 pN. With increasing pulling rate up to 5 µm/s, a pronounced maximum in the binding force is observed at pH 7.4 and its magnitude reaches ~150-200 pN at 5 µm/s. This maximum vanishes for experiments carried out at 10 and 20 µm/s pulling rates, and the binding force then reaches a pH-independent value of ~65-100 pN under such conditions. Overall, the results of Figure 5 indicate that the FimH-mannose binding force strongly depends on solution pH for some critical values of the pulling rate (here 5 µm/s). For all other values tested in this work, the FimH-mannose binding force is minimal, quasi pH-independent (50-75 pN) and nearly independent of the retraction rate.

The pH value corresponding to pronounced maximum in binding force for a pulling rate of 5 µm/s, identifies to the pH marking a maximum unwinding distance of the fimbrial rod (Figure 4). Besides, we observed that the persistence length reflecting the FimH-mannose flexibility is independent of pH and pulling rate (Figure 3a,b and Figure S2), which suggests that the conformation of the FimH adhesin remains identical regardless the values of the stretching rate and the solution pH. Altogether, these elements indicate that the variations of the maximal fimbriae elongation distance with pH and pulling rate (Figure 4) is related to the only modification of the molecular interactions or connections between FimA units within the fimbrial rod.

In addition, Figure 5 illustrates that if the 'catch bond effect' takes place, it only does within the pH range 5 to 9 for pulling rates lower than 10 μm/s. This suggests that beyond a critical value of the pulling rate (*i.e.* 10 μm/s), the FimH-mannose binding is attenuated following dynamic effects, *i.e.* the bond between the fimbriae lectin ending part and the mannosyl residue has no longer time to fully settle. Overall, two important processes concomitantly take place at neutral pH when unwinding fimbria: a weakening of the FimA-FimA interaction forces (Figure 4) and an increased FimH-mannose interaction (Figure 5). The former effect was suggested in Rangel *et al.*[48] on piliated bacteria subjected to various flow rates. This study indicated that the mechanical and functional properties of the pili, in particular, their extensibility, may reduce tension upon alignment of their structure along the flow direction. In turn, this uncoiling of the pili modifies the force to be applied for detaching the terminal adhesion from the surface [48], which is pretty much in line with the results of Figures 4 and 5.

Effect of pH on electrokinetics of bacterial cells.

In order to better understand the effect of pH on the cell wall properties of *E. coli*, we performed electrophoretic mobility measurements in M63B1glu medium over the pH range 3 to 9 for the strain E2146 (constitutively expressing type 1 fimbriae).

As detailed elsewhere,[25] these macroscopic measurements allow the evaluation of key electrostatic and structural properties averaged over the entire soft surface structure carried by the cell. As such, electrokinetics cannot be exploited to extract molecular details pertaining to the only FimH-mannose interaction but it is however relevant for understanding how the surface charge density of the bacterial cell wall structure is modified by pH and thus how the FimA-FimA interactions may potentially be involved in the fimbrial unwinding process. The electrophoretic mobility results were systematically compared to those obtained for the reference strain E2152 that does not produce type 1 fimbriae and does not agglutinate yeast

cells regardless the pH medium (see next section). The dependence of the electrophoretic mobility of the bacterial strains E2152 and E2146 are reported in Figure 6a. For all strains, μ is negative, as expected for biological particles,[49] and it increases in absolute value with increasing pH following the deprotonation of ionogenic groups distributed throughout the cell wall structures. The mobility of E2152 cells reaches a plateau value of about 1.5×10^{-8} $m^2.s^{-1}.V^{-1}$ for pH values in the range 6 to 8. The electrophoretic mobility of E2146 cells significantly differ from that of E2152. In details, the mobility increases in magnitude with pH, reaches a constant value in the pH range 6 to 7.5 and increases again for pH larger than 8. In addition, under fixed pH condition, the mobility of E2146 strain is lower in magnitude as compared to that of the bacterial reference strain E2152 except at pH >8.5 where mobilities of both strains are similar. This trend is explained by an increased friction force exerted by the loose fimbrial appendage structure on the electroosmotic flow, [49] thereby reducing the mobility of E2146 as compared to that of E2152 (Figure 6). With regard to E2146 strain, the increase in mobility values with pH basically corresponds to an increase of the negative charge density within the fimbrial surface structure surrounding the cell wall.

The differential mobility Δμ reported in Figure 6b was evaluated from the difference between the electrophoretic mobilities of E2146 and of the reference bacteria (E2152) determined under similar pH condition. Because of the strain constructions, Δμ may be related to the sole electrohydrodynamic features pertaining to the fimbrial structure. In details, Δμ exhibits a non monotonous behaviour with varying pH. It decreased by a factor 4 between pH 3 and 5.5, the latter pH value corresponding to the FimA isoelectric point (denoted as pI(FimA). Then, we observed a local maximum in Δμ at pH 7. With further increasing pH, Δμ tended to zero and the Δμ value at pH 7.5 (*i.e.* at the FimH isoelectric point (pI(FimH)) is identical to that at pH 5.5, *i.e.* at pI(FimA) . The fact that the Δμ tends to zero for pH larger than pI(FimA) and pI(FimH) means that the fully expressed charge of the fimbriae layer at the cell surface under

such pH conditions counteracts the friction force exerted by the cell surface appendages on the electroosmotic flow so that, in turn, the mobility of E2146 strain is identical to that of the reference strain E2152 at high pH. The presence of a maximum in Δμ at pH 7 likely originates from the combination of two processes: first the important increase of the charges on the FimA units (at pH values around pI(FimA)) leads to an increase of the local repulsive electrostatic interactions between adjacent fimbriae. This will in turn likely induce their extension (swelling) even though the latter is expected to be limited under the salinity conditions of the experiments. Nevertheless, even such a slight extension of the fimbrial structure can dramatically impact cell electrophoretic mobility.[48] *In fine*, the mobility of E2146 is reduced due to the larger friction exerted by the structure. Once the FimH charge is expressed the fimbrial filaments being already stretched, the electrophoretic mobility will increase again in absolute value and eventually return to the level of that measured for E2152. Macroscopic measurements of bacterial surface structure properties, as obtained from electrokinetics, therefore support the importance of the electrostatic interactions within the fimbrial structure and, in particular, the key role played by the solution pH on their extension, as evidenced by the detailed molecular AFM analysis. The maximum in Δμ commented above and observed in the pH window ~5 to ~8 well matches that obtained for the maximal extension of fimbriae (Figure 4), thus revealing a role played by electrostatics in the non-monotonous behavior measured for the fimbriae flexibility under the action of external forces.

Correlation between AFM analysis and bacterial yeast agglutination.

In order to evaluate the relevance -at a macroscopic scale- of the observed impact of solution pH on the adhesion force between FimH and mannose (Figure 5), we performed yeast agglutination assays (Figure 7). By virtue of interaction between FimH and mannosylated proteins located at the surface of yeast cells, *E. coli* expressing type 1 fimbriae has the

capacity to interact simultaneously with several yeast cells, thus leading to yeast agglutination. Using this assay, the level of yeast agglutination can be directly correlated to the efficient binding between FimH and mannose. Interestingly, we obtained an optimum in yeast agglutination at pH 5, 6 and 7 while weaker agglutination was detected at pH 3, 8 and 9 (Figure 7). This result strongly supports the dependence of the FimH-mannose binding force on pH at pulling rates lower than 5 μm/s as obtained from AFM analysis. It further confirms that neutral pH conditions lead to maximum interaction between FimH and mannose under moderate pulling rates that are in line with Brownian encounter/collision between bacteria and yeasts.

A correlation may be also further drawn between our molecular FimH-mannose interaction measurements and the adhesion behavior of *E. coli* under physiological conditions when present in the gastro-intestinal and urinary tracts of human. Indeed, *E. coli* is not known as an efficient colonizer of the stomach where the pH is very acidic, which is in line with the low adhesion force measured in our study under such pH condition and with a reduced expression of type 1 fimbriae at such extreme pH value.[50] It is further accepted that type 1 fimbriae efficiently bind to colonic and ileal enterocytes [51] thereby suggesting a type 1 fimbriae-mediated colonization of mammals gut. Accordingly, *E. coli* K1 and APEC type 1 fimbriae have been shown to be necessary for mouse and chicken intestinal colonization, respectively.[52, 53] For humans, the pH in the gut is 6 in the duodenum part, 7.4 in the ileum, 5.7 in the caecum and 6.7 in the rectum [54, 55], *i.e.* the pH value is compatible with that reported here where there is a maximum in adhesion of type 1 fimbriae. Additionally, in the urinary tract, pH of urine is generally larger than 5.0 [56, 57] and it thus again corresponds to optimal condition for strong type 1 fimbriae-mediated cell adhesion and colonization of the bladder.

Conclusions

The results reported in this work demonstrate that type 1 fimbriae are dynamic structures whose flexibility and binding force to mannosylated surfaces can be modulated with changing external shear forces and solution pH conditions. Using single-molecule force and dynamic force spectroscopies, we found that this modulation is mostly governed by both FimA-FimA and FimH-mannose interactions. The combination of these interactions was evidenced from the analysis of the maximal fimbriae extension determined with using live bacterial cells investigated under various pH conditions. We further found that fimbrial unwinding that reflects the strengths of the FimA-FimA interactions was dramatically decreased by a factor 5 and 25 for pulling rates larger than a given corner velocity and for pH values outside the range 5 to 8, respectively. Furthermore, dynamic force spectroscopy analyses performed with AFM probes specific to FimH revealed the occurrence of a minimal FimH-mannose binding force of about 50-75 pN that is quasi-independent of the applied pulling force and the pH conditions. In addition, we observed that for increasing pulling rate up to 5 µm/s, the FimH-mannose interaction force is maximal at pH 7.4 with a magnitude of ~150-200 pN. Finally, beyond a critical value of the pulling rate of about 10 µm/s, this maximum in FimH-mannose interaction force disappears. This suggests that that may the 'catch bond effect' take place, it does only within the pH range 5 to 9 and for pulling rates lower than 10 µm/s.

The results derived from molecular AFM analysis are supported by the macroscopic results obtained fromyeast agglutination assays and electrophoretic mobility measurements performed on bacteria over-expressing type 1 fimbriae under different pH conditions. In particular, we evidenced an optimum of yeast agglutination in the pH range 5 to 7, in line with the maximum detected by AFM for the binding force between FimH and mannose at neutral pH under moderate applied pulling rate. Moreover, electrokinetic measurements

strongly point out the importance of pH conditions for understanding and explaining bacterial adhesion under various and changing environmental conditions.

Acknowledgement

C.S. is supported by a MENESR (Ministère Français de l'Éducation Nationale, de l'Enseignement Supérieur et de la Recherche) fellowship. A.C., C.B and J-M.G. are supported by the Institut Pasteur and the French Government's Investissement d'Avenir program, Laboratoire d'Excellence "Integrative Biology of Emerging Infectious Diseases" (grant n°ANR-10-LABX-62-IBEID).

References

1. Camesano, T. A.; Liu, Y. T.; Datta, M., Measuring bacterial adhesion at environmental interfaces with single-cell and single-molecule techniques. Advances in Water Resources 30, 1470-1491 **(2007)**.

2. Kline, K. A.; Falker, S.; Dahlberg, S.; Normark, S.; Henriques-Normark, B., Bacterial Adhesins in Host-Microbe Interactions. Cell Host Microbe 5, 580-592 **(2009)**.

3. Proft, T.; Baker, E. N., Pili in Gram-negative and Gram-positive bacteria - structure, assembly and their role in disease. Cell. Mol. Life Sci. 66, 613-635 **(2009)**.

4. Wiles, T. J.; Kulesus, R. R.; Mulvey, M. A., Origins and virulence mechanisms of uropathogenic *Escherichia coli*. Exp. Mol. Pathol. 85, 11-19 **(2008)**.

5. Andersson, M.; Uhlin, B. E.; Fallman, E., The biomechanical properties of E-coli Pili for urinary tract attachment reflect the host environment. Biophys. J. 93, 3008-3014 **(2007)**.

6. Wu, X. R.; Sun, T. T.; Medina, J. J., In vitro binding of type 1-fimbriated *Escherichia coli* to uroplakins Ia and Ib: relation to urinary tract infections. Proc Natl Acad Sci USA 93, 9630-5 **(1996)**.

7. Klemm, P.; Christiansen, G., Three fim genes required for the regulation of length and mediation of adhesion of *Escherichia coli* type 1 *fimbriae*. Mol Gen Genet 208, 439-45 **(1987)**.

8. Mu, X. Q.; Bullitt, E., Structure and assembly of P-pili: A protruding hinge region used for assembly of a bacterial adhesion filament. Proc. Natl. Acad. Sci. U. S. A. 103, 9861-9866 **(2006)**.

9. Lane, M. C.; Mobley, H. L. T., Role of P-fimbrial-mediated adherence in pyelonephritis and persistence of uropathogenic Escherichia coli (UPEC) in the mammalian kidney. Kidney Int. 72, 19-25 **(2007)**.

10. Dufrêne, Y. F., Using nanotechniques to explore microbial surfaces. Nature Reviews: Microbiology 2, 451-460 **(2004)**.

11. Dufrêne, Y. F., Atomic force microscopy and chemical force microscopy of microbial cells. Nat. Protoc. 3, 1132-8 **(2008)**.

12. Francius, G.; Lebeer, S.; Alsteens, D.; Wildling, L.; Gruber, H. J.; Hols, P.; De Keersmaecker, S.; Vanderleyden, J.; Dufrêne, Y. F., Detection, localization, and conformational analysis of single polysaccharide molecules on live bacteria. ACS Nano 2, 1921-9 **(2008)**.

13. Dupres, V.; Alsteens, D.; Andre, G.; Dufrene, Y. F., Microbial nanoscopy: a closer look at microbial cell surfaces. Trends Microbiol. 18, 397-405 **(2010)**.

14. Hinterdorfer, P.; Dufrêne, Y. F., Detection and localization of single molecular recognition events using atomic force microscopy. Nat. Methods 3, 347-355 **(2006)**.

15. Alsteens, D.; Garcia, M. C.; Lipke, P. N.; Dufrêne, Y. F., Force-induced formation and propagation of adhesion nanodomains in living fungal cells. Proc. Natl. Acad. Sci. U. S. A. 107, 20744-20749 **(2010)**.

16. Bjornham, O.; Nilsson, H.; Andersson, M.; Schedin, S., Physical properties of the specific PapG-galabiose binding in E-coli P pili-mediated adhesion. European Biophysics Journal with Biophysics Letters 38, 245-254 **(2009)**.

17. Andersson, M.; Fallman, E.; Uhlin, B. E.; Axner, O., Dynamic force spectroscopy of E coli P pili. Biophys. J. 91, 2717-2725 **(2006)**.

18. Axner, O.; Andersson, M.; Bjornham, O.; Castelain, M.; Klinth, J.; Koutris, E.; Schedin, S., Assessing Bacterial Adhesion on an Individual Adhesin and Single Pili Level Using Optical Tweezers. In Bacterial Adhesion: Chemistry, Biology and Physics, Linke, D.; Goldman, A., Eds. Vol. 715, pp 301-313 **(2011)**.

19. Castelain, M.; Ehlers, S.; Klinth, J.; Lindberg, S.; Andersson, M.; Uhlin, B. E.; Axner, O., Fast uncoiling kinetics of F1C pili expressed by uropathogenic Escherichia coli are revealed on a single pilus level using force-measuring optical tweezers. European Biophysics Journal with Biophysics Letters 40, 305-316 **(2011)**.

20. Bullitt, E.; Makowski, L., Structural polymorphism of bacterial adhesion Pili. Nature 373, 164-167 **(1995)**.

21. Andersson, M.; Bjornham, O.; Svantesson, M.; Badandah, A.; Uhlin, B. E.; Bullitt, E., A Structural Basis for Sustained Bacterial Adhesion: Biomechanical Properties of CFA/I Pili. J. Mol. Biol. 415, 918-928 **(2012)**.

22. Li, Y. F.; Poole, S.; Nishio, K.; Jang, K.; Rasulova, F.; McVeigh, A.; Savarino, S. J.; Xia, D.; Bullitt, E., Structure of CFA/I fimbriae from enterotoxigenic Escherichia coli. Proc. Natl. Acad. Sci. U. S. A. 106, 10793-10798 **(2009)**.

23. Yakovenko, O.; Sharma, S.; Forero, M.; Tchesnokova, V.; Aprikian, P.; Kidd, B.; Mach, A.; Vogel, V.; Sokurenko, E.; Thomas, W. E., FimH forms catch bonds that are enhanced by mechanical force due to allosteric regulation. J. Biol. Chem. 283, 11596-11605 **(2008)**.

24. Polyakov, P.; Soussen, C.; Duan, J. B.; Duval, J. F. L.; Brie, D.; Francius, G., Automated Force Volume Image Processing for Biological Samples. PLoS One 6, e18887 **(2011)**.

25. Francius, G.; Polyakov, P.; Merlin, J.; Abe, Y.; Ghigo, J. M.; Merlin, C.; Beloin, C.; Duval, J. F. L., Bacterial Surface Appendages Strongly Impact Nanomechanical and Electrokinetic Properties of Escherichia coli Cells Subjected to Osmotic Stress. PLoS One 6, e20066 **(2011)**.

26. Da Re, S.; Le Quere, B.; Ghigo, J. M.; Beloin, C., Tight modulation of *Escherichia coli* bacterial biofilm formation through controlled expression of adhesion factors. Appl. Environ. Microbiol. 73, 3391-3403 **(2007)**.

27. Korea, C. G.; Badouraly, R.; Prévost, M. C.; Ghigo, J. M.; Beloin, C., *E. coli* K-12 possesses multiple cryptic but functional chaperone-usher *fimbriae* with distinct surface specificities. Environ. Microbiol. 12, 1957-1977 **(2010)**.

28. Hasman, H.; Schembri, M. A.; Klemm, P., Antigen 43 and type 1 fimbriae determine colony morphology of *Escherichia coli* K-12. J. Bacteriol. 182, 1089-1095 **(2000)**.

29. Francius, G.; Alsteens, D.; Dupres, V.; Lebeer, S.; De Keersmaecker, S.; Vanderleyden, J.; Gruber, H. J.; Dufrêne, Y. F., Stretching polysaccharides on live cells using single molecule force spectroscopy. Nat. Protoc. 4, 939-946 **(2009)**.

30. Mol, O.; Oudega, B., Molecular and structural aspects of fimbriae biosynthesis and assembly in *Escherichia coli*. FEMS Microbiol. Rev. 19, 25-52 **(1996)**.

31. Hahn, E.; Wild, P.; Hermanns, U.; Sebbel, P.; Glockshuber, R.; Häner, M.; Taschner, N.; Burkhard, P.; Aebi, U.; Müller, S. A., Exploring the 3D molecular architecture of *Escherichia coli* type 1 *pili*. J. Mol. Biol. 323, 845-57 **(2002)**.

32. Vogel, A.; Elmabsout, B.; Gintz, D., Modelling of urine flow in an ureteral bolus. C. R. Mec. 332, 737-742 **(2004)**.

33. Forero, M.; Yakovenko, O.; Sokurenko, E. V.; Thomas, W. E.; Vogel, V., Uncoiling mechanics of *Escherichia coli* type I *fimbriae* are optimized for catch bonds. PLoS Biol. 4, 1509-1516 **(2006)**.

34. Thomas, W. E.; Vogel, V.; Sokurenko, E., Biophysics of catch bonds. In Annual Review of Biophysics, Vol. 37, pp 399-416 **(2008)**.

35. Root, D. D.; Yadavalli, V. K.; Forbes, J. G.; Wang, K., Coiled-Coil Nanomechanics and Uncoiling and Unfolding of the Superhelix and α-Helices of Myosin. Biophys. J. 90, 2852-2866 **(2006)**.

36. Kajava, A. V.; Cheng, N.; Cleaver, R.; Kessel, M.; Simon, M. N.; Willery, E.; Jacob-Dubuisson, F.; Locht, C.; Steven, A. C., Beta-helix model for the filamentous haemagglutinin adhesin of *Bordetella pertussis* and related bacterial secretory proteins. Mol. Microbiol. 42, 279-292 **(2001)**.

37. Yoder, M. D.; Keen, N. T.; Jurnak, F., New domain motif - The structure of pectate lyase-C, a secreted plant virulence factor. Science 260, 1503-1507 **(1993)**.

38. Ainavarapu, R. K.; Brujic, J.; Huang, H. H.; Wiita, A. P.; Lu, H.; Li, L. W.; Walther, K. A.; Carrion-Vazquez, M.; Li, H. B.; Fernandez, J. M., Contour length and refolding rate of a small protein controlled by engineered disulfide bonds. Biophys. J. 92, 225-233 **(2007)**.

39. Grater, F.; Heider, P.; Zangi, R.; Berne, B. J., Dissecting entropic coiling and poor solvent effects in protein collapse. J. Am. Chem. Soc. 130, 11578-11579 **(2008)**.

40. Tobi, D.; Elber, R., Distance-dependent, pair potential for protein folding: Results from linear optimization. Proteins-Structure Function and Genetics 41, 40-46 **(2000)**.

41. Rheinlaender, J.; Grabner, A.; Ott, L.; Burkovski, A.; Schaffer, T. E., Contour and persistence length of Corynebacterium diphtheriae pili by atomic force microscopy. European Biophysics Journal with Biophysics Letters 41, 561-570 **(2012)**.

42. Puorger, C.; Vetsch, M.; Wider, G.; Glockshuber, R., Structure, Folding and Stability of FimA, the Main Structural Subunit of Type 1 Pili from Uropathogenic Escherichia coli Strains. J. Mol. Biol. 412, 520-535 **(2011)**.

43. Andersson, M.; Axner, O.; Almqvist, F.; Uhlin, B. E.; Fallman, E., Physical properties of biopolymers assessed by optical tweezers: Analysis of folding and refolding of bacterial pili. ChemPhysChem 9, 221-235 **(2008)**.

44. Miller, E.; Garcia, T.; Hultgren, S.; Oberhauser, A. F., The mechanical properties of *E. coli* type 1 pili measured by atomic force microscopy techniques. Biophys. J. 91, 3848-56 **(2006)**.

45. Klinth, J. E.; Castelain, M.; Uhlin, B. E.; Axner, O., The Influence of pH on the Specific Adhesion of P Piliated Escherichia coli. PLoS One 7, e38548 **(2012)**.

46. Aprikian, P.; Interlandi, G.; Kidd, B. A.; Le Trong, I.; Tchesnokova, V.; Yakovenko, O.; Whitfield, M. J.; Bullitt, E.; Stenkamp, R. E.; Thomas, W. E.; Sokurenko, E. V., The Bacterial Fimbrial Tip Acts as a Mechanical Force Sensor. PLoS Biol. 9, e1000617 **(2011)**.

47. Bosshard, H. R.; Marti, D. N.; Jelesarov, I., Protein stabilization by salt bridges: concepts, experimental approaches and clarification of some misunderstandings. J. Mol. Recognit. 17, 1-16 **(2004)**.

48. Rangel, D. E.; Marin-Medina, N.; Castro, J. E.; Gonzalez-Mancera, A.; Forero-Shelton, M., Observation of Bacterial Type I Pili Extension and Contraction under Fluid Flow. PLoS One 8, **(2013)**.

49. Duval, J. F. L.; Gaboriaud, F., Progress in electrohydrodynamics of soft microbial particle interphases. Curr. Opin. Colloid Interface Sci. 15, 184-195 **(2010)**.

50. Schwan, W. R.; Lee, J. L.; Lenard, F. A.; Matthews, B. T.; Beck, M. T., Osmolarity and pH growth conditions regulate fim gene transcription and type 1 pilus expression in uropathogenic Escherichia coli. Infect. Immun. 70, 1391-1402 **(2002)**.

51. Adlerberth, I.; Hanson, L. A.; Svanborg, C.; Svennerholm, A. M.; Nordgren, S.; Wold, A. E., Adhesins of *Escherichia coli* associated with extraintestinal pathogenicity confer binding to colonic epithelial cells. Microbial Pathogenesis 18, 373-385 **(1995)**.

52. La Ragione, R. M.; Cooley, W. A.; Woodward, M. J., The role of fimbriae and flagella in the adherence of avian strains of Escherichia coli O78 : K80 to tissue culture cells and tracheal and gut explants. J. Med. Microbiol. 49, 327-338 **(2000)**.

53. Martindale, J.; Stroud, D.; Moxon, E. R.; Tang, C. M., Genetic analysis of Escherichia coli K1 gastrointestinal colonization. Mol. Microbiol. 37, 1293-1305 **(2000)**.

54. Fallingborg, J., Intraluminal pH of the human gastrointestinal tract. Danish Medical Bulletin 46, 183-196 **(1999)**.

55. Nugent, S. G.; Kumar, D.; Rampton, D. S.; Evans, D. F., Intestinal luminal pH in inflammatory bowel disease: possible determinants and implications for therapy with aminosalicylates and other drugs. Gut 48, 571-577 **(2001)**.

56. Asscher, A. W.; Sussman, M.; Waters, W. E.; Davis, R. H.; Chick, S., Urine as a medium for bacterial growth. Lancet 2, 1037-1041 **(1966)**.

57. Waters, W. E.; Sussman, M.; Asscher, A. W., Community study of urinary pH and osmolarity. British Journal of Preventive & Social Medicine 21, 129-132 **(1967)**.

Tables

Table 1.

Values for the rupture forces corresponding to the main modes of the statistical distribution given in Figure 2c. Corresponding conformational parameters (persistence and contour lengths, l_p and L_c, respectively) as derived from WLC model (eq 1). Data were extracted from a 5μm×5μm Force Volume Image (FVI) consisting of 1024 force curves recorded on several bacteria at pH 7 and for a pulling rate of 2 μm/s.

Worm Like Chain model (pH 7, v = 2 μm/s)		
Rupture forces (pN)	**l_p (nm)**	**L_c (nm)**
95 ± 25	0.05 ± 0.03	367 ± 241
169 ± 21	0.21 ± 0.07	1715 ± 412
244 ± 69	--	5873 ± 3792

Table 2.

Values for the rupture forces corresponding to the main modes of the statistical distribution given in Figure 2d. Corresponding conformational parameters (persistence and contour lengths, l_p and L_c, respectively) as derived from WLC model (eq 1). Data were extracted from a 5μm×5μm Force Volume Image (FVI) consisting of 1024 force curves recorded on several bacteria at pH 7 and for a pulling rate of 20 μm/s.

Worm Like Chain model (pH 7, v = 20 μm/s)		
Rupture forces (pN)	**l_p (nm)**	**L_c (nm)**
70 ± 19	0.04 ± 0.03	453 ± 330
141 ± 43	0.22 ± 0.11	3915 ± 677
281 ± 140	--	--

Table S1.

Average maximal fimbriae unwinding calculated from the last rupture distance on the force curves showing adhesive events. Each average value was derived from a Force Volume Image of 1024 force curves recorded on single bacteria at pH 3, 5, 7 and 8 for a pulling rate of 5 µm/s.

Maximal fimbriae elongation in nm (v = 2 µm/s)			
pH = 3	**pH = 5**	**pH = 7**	**pH = 8**
387 ± 213	1634 ± 1082	8487 ± 1294	607 ± 411
1966 ± 304	--	--	1838 ± 284

Figure captions

Figure 1.

a) Schematic representation of type 1 fimbriae anchored at the outer membrane of *E. coli* cell.

b) Deflection and adhesion images of single E 2146 mutant bacteria constitutively expressing type 1 fimbriae on its cell wall.

Figure 2.

(a, b) Typical force-curves corresponding to multiple and single type 1 fimbriae molecular uncoiling for retraction speed of 2 and 20 μm/s at pH 7. Black circles correspond to experimental retraction force curves and red lines correspond to WLC theoretical fittings.

(c, d) Statistical distribution of FimH-mannose binding rupture force for pulling rate of 2 and 20 μm/s at pH 7.

Figure 3.

(a, b) Statistical analysis of the persistence length obtained from WLC modeling for pulling rate of 2 (panel a) and 20 μm/s (panel b) at pH 7.

(c, d) Statistical analysis of the contour length obtained from WLC modeling for pulling rate of 2 (panel c) and 20 μm/s (panel d) at pH 7.

Figure 4.

Dependence of the maximal type 1 fimbriae elongation obtained by Single Molecule Force experimentson pH for pulling rates of 0.5 μm/s (a), 1 μm/s (b), 2 μm/s (c), 5 μm/s (d), 10 μm/s (e) and 20 μm/s (f). Maximal elongations were evaluated from the last rupture distance in the force curves recorded under the conditions described above.

Figure 5.

Dependence of FimH-mannose binding force obtained by Single Molecule Force experiments on pH for pulling rates of 0.5 µm/s (a), 1 µm/s (b), 2 µm/s (c), 5 µm/s (d), 10 µm/s (e) and 20 µm/s (f). FimH-mannose binding force corresponds to the last rupture force event in the force curves recorded under the conditions described above.

Figure 6.

(a) pH-dependence of the electrophoretic mobility for E2146 and E2152 in M63B1glu medium.

(b) Differential mobility evaluatedfrom the difference between electrophoretic mobility reported in (a) forE2146 and E2152.

Figure 7.

Yeast agglutination assay for E2146 performed over the pH range 3 to 9. The strain E2152 is deleted for type 1 fimbriae *fim* operon and it thus does not agglutinate yeast cells.

Figure S1.

Scheme of single-molecule force spectroscopy experiment performed on live bacterial cell.

Figure S2.

Retraction force curves recorded for pulling rate of 2 µm/s at pH 3 (a), pH 5 (b), pH 6 (c), pH 7 (d), pH 8 (e) and pH 9 (f). Black circles correspond to experimental retraction force curves and red lines correspond to WLC theoretical fittings.

Figure S3.

Statistical distributions of the persistence length for retraction rates of 2, 5, 10 and 20 μm/s at pH 3, 5, 6, 7 and 8. Values were obtained from analysis of Force Volume Images of 1024 force curves recorded on single bacteria.

Figure S4.

(a, b) Statistical distribution of the maximal type 1 fimbriae elongation obtained for a pulling rate of 5 μm/s at pH 3 and 5.

(c, d) Statistical distribution of the maximal type 1 fimbriae elongation obtained for a pulling rate of 5 μm/s at pH 7 and 8.

Values were calculated from a Force Volume Images of 1024 force curves recorded on single bacteria.

Figure S5.

Scheme illustrating the impact of pulling rate on the unwinding of type 1 fimbriae.

Figure S6.

Scheme illustrating the impact of pH on the unwinding and flexibility of type 1 fimbriae.

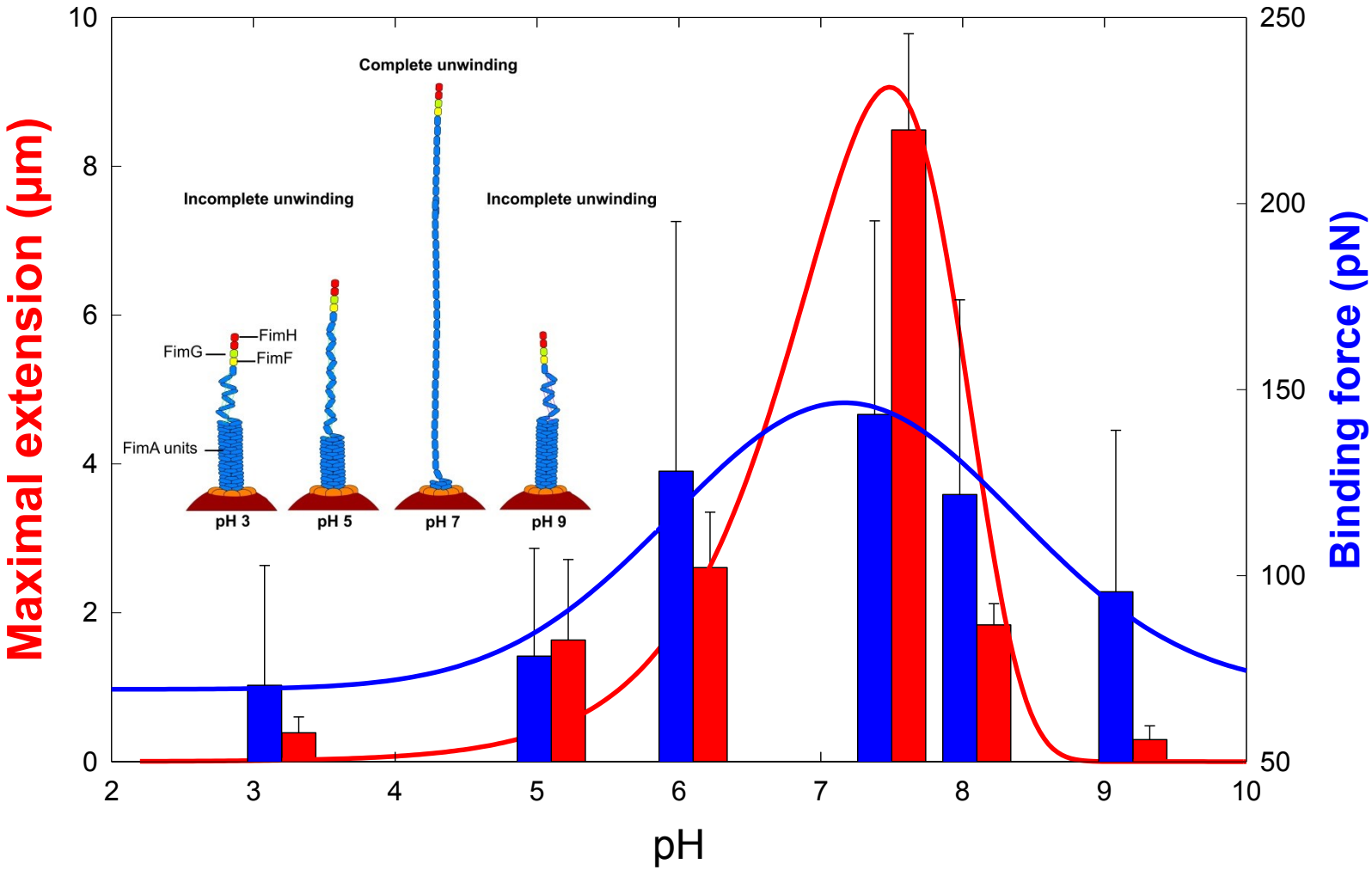
Maximal extension (μm)
Binding force (pN)
pH
Complete unwinding
Incomplete unwinding
Incomplete unwinding
FimH
FimG
FimF
FimA units
pH 3
pH 5
pH 7
pH 9

TOC

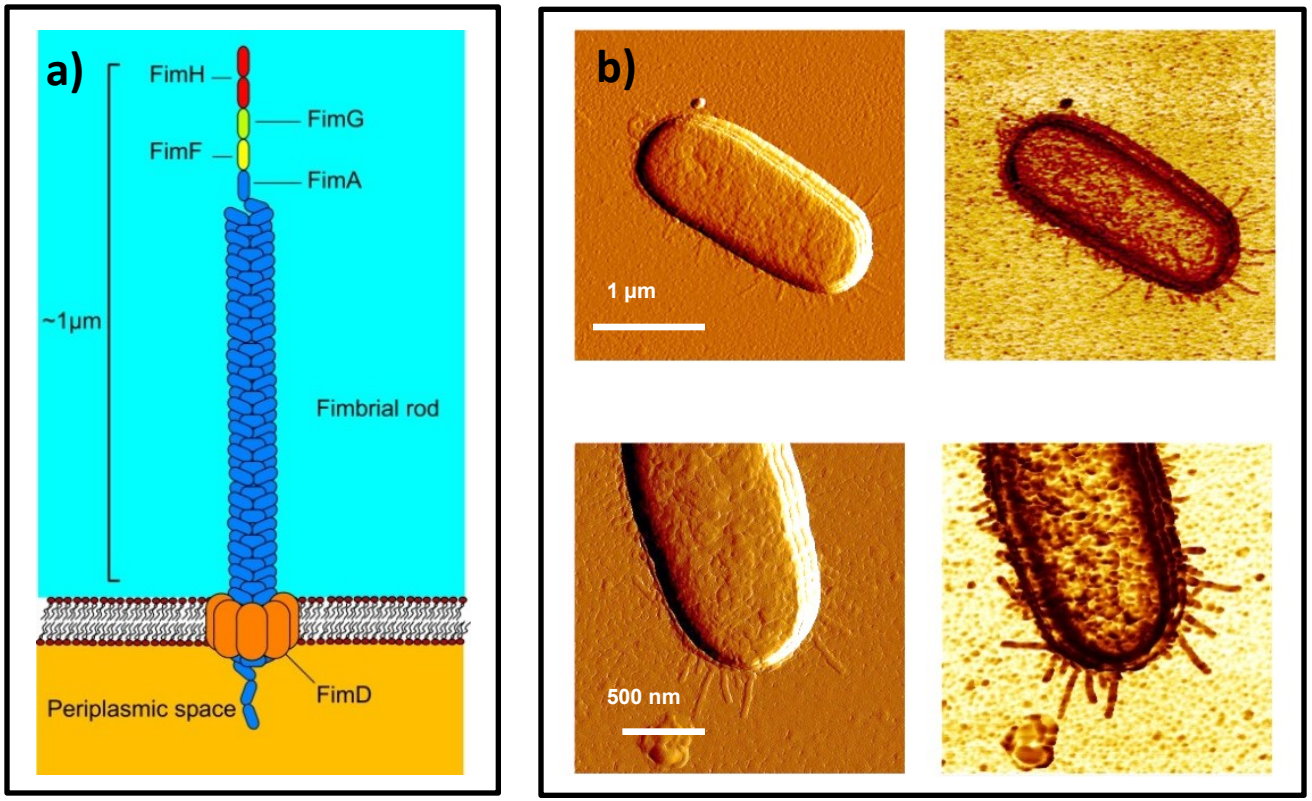
a)
FimH
FimG
FimF
FimA
~1µm
Fimbrial rod
Periplasmic space
FimD
b)
1 µm
500 nm

Figure 1.

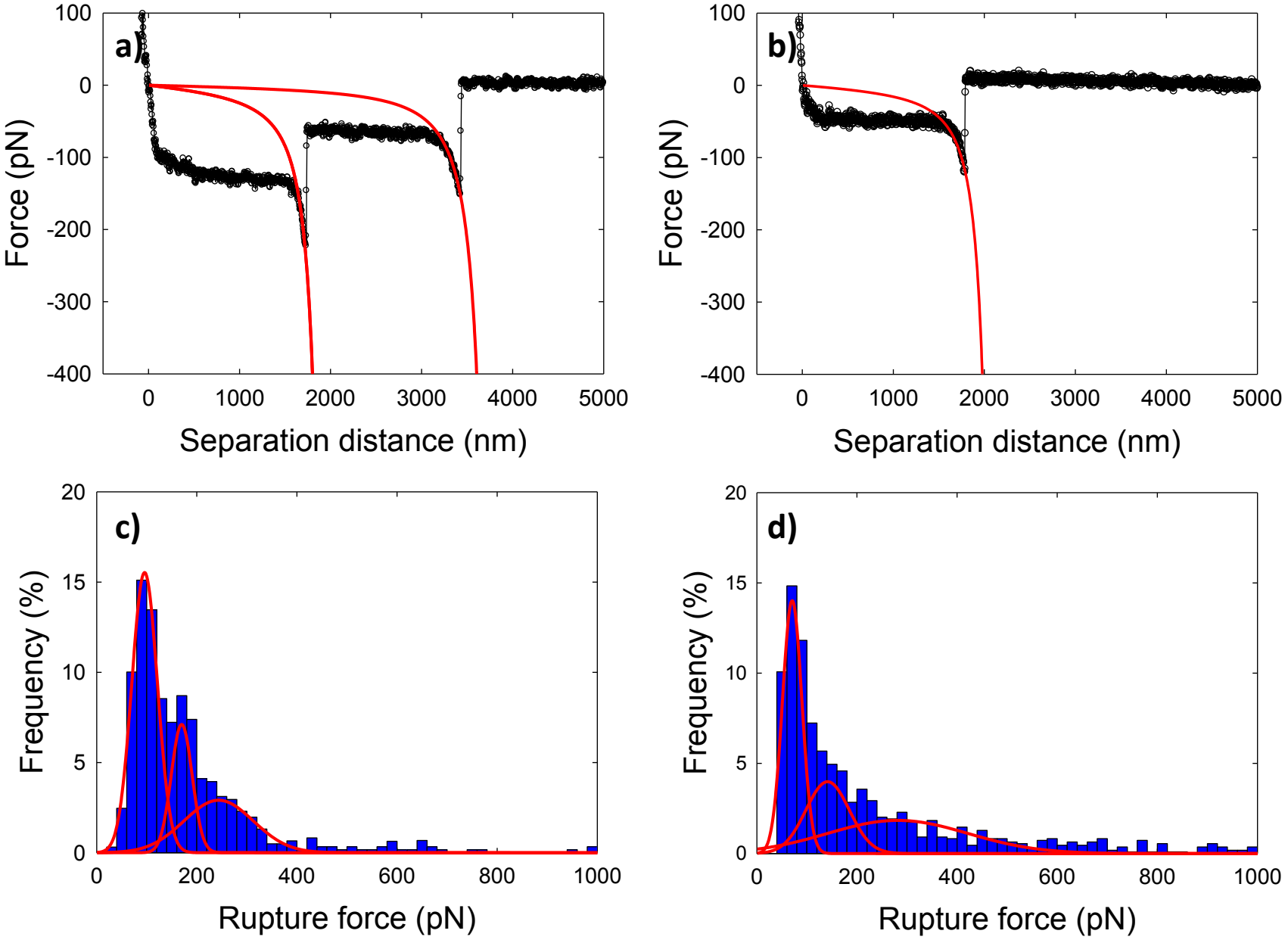
a)
b)
c)
d)
Force (pN)
Separation distance (nm)
Frequency (%)
Rupture force (pN)
100
0
-100
-200
-300
-400
0
1000
2000
3000
4000
5000
20
15
10
5
0
200
400
600
800
1000

Figure 2.

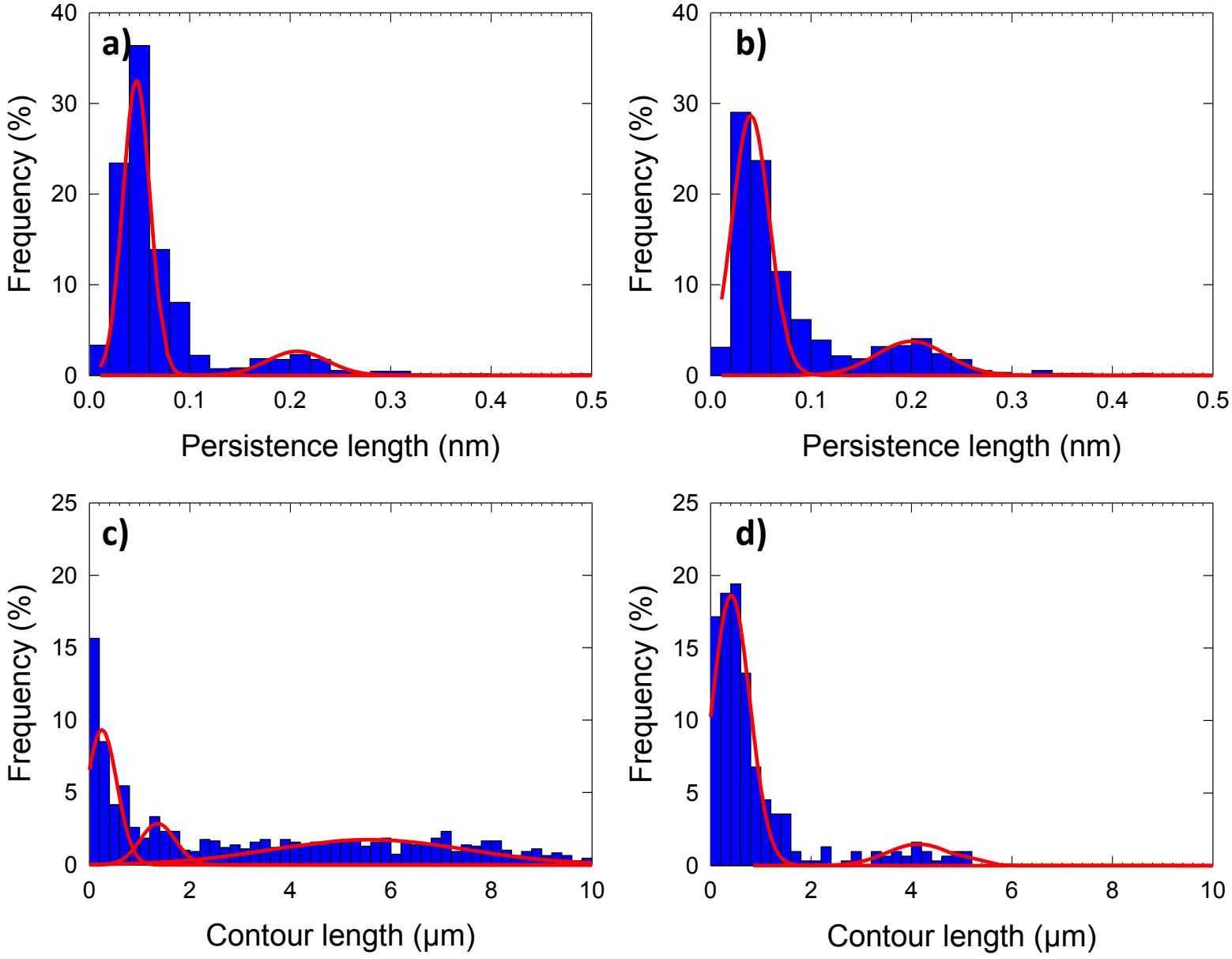
a)
b)
c)
d)
Frequency (%)
Persistence length (nm)
Contour length (μm)
0
10
20
30
40
0.0
0.1
0.2
0.3
0.4
0.5
5
15
25
2
4
6
8
10

Figure 3.

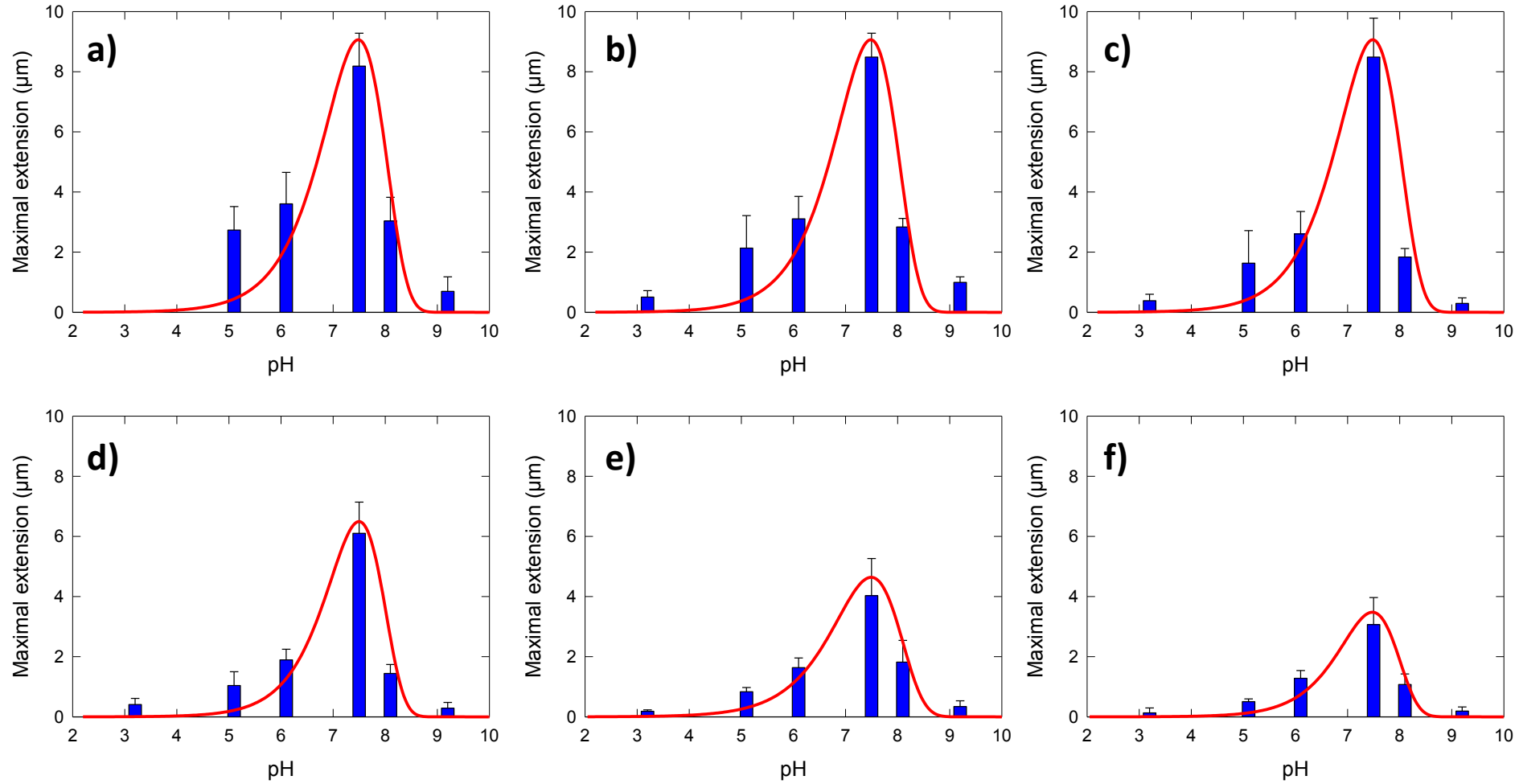

Figure 4.

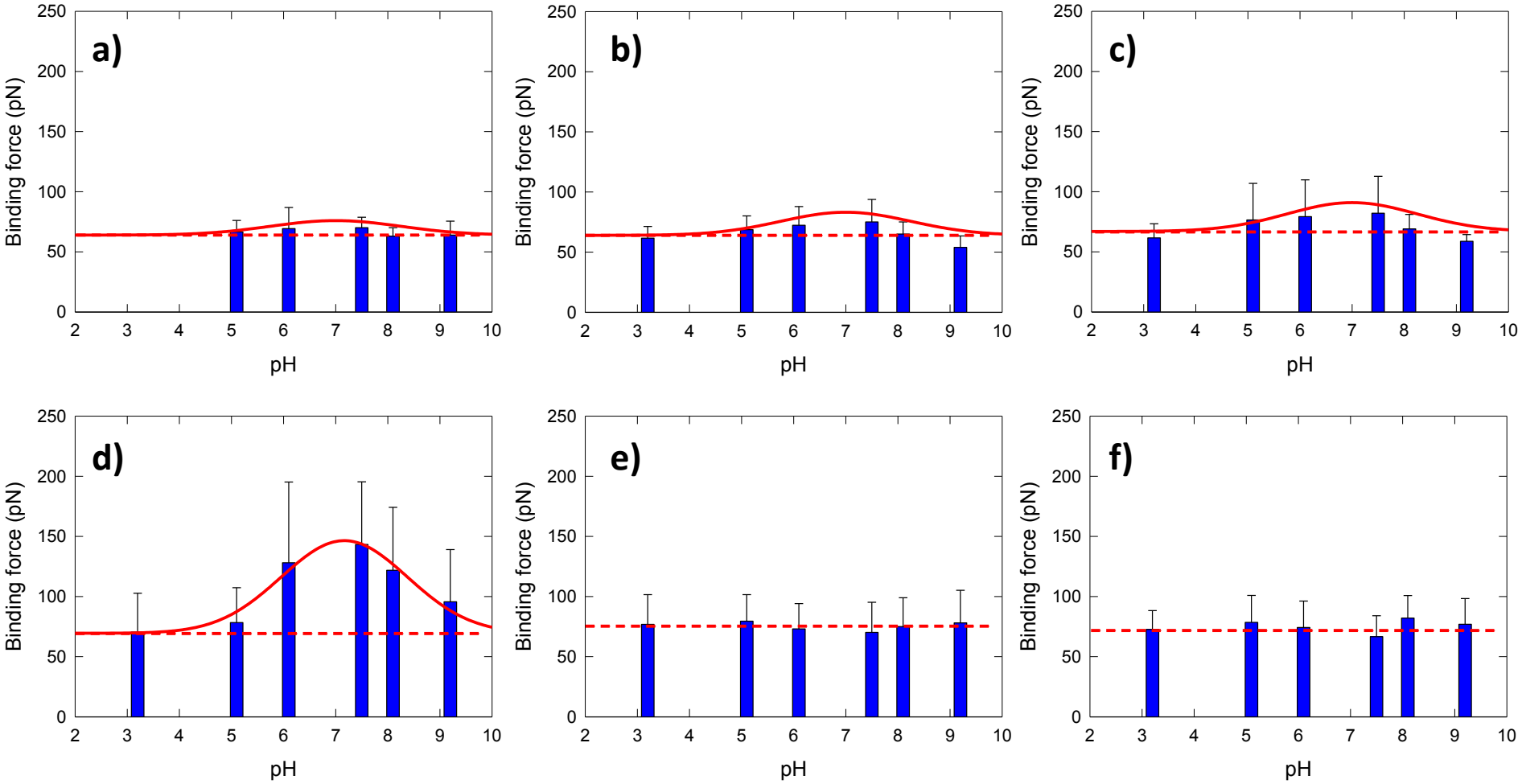

Figure 5.

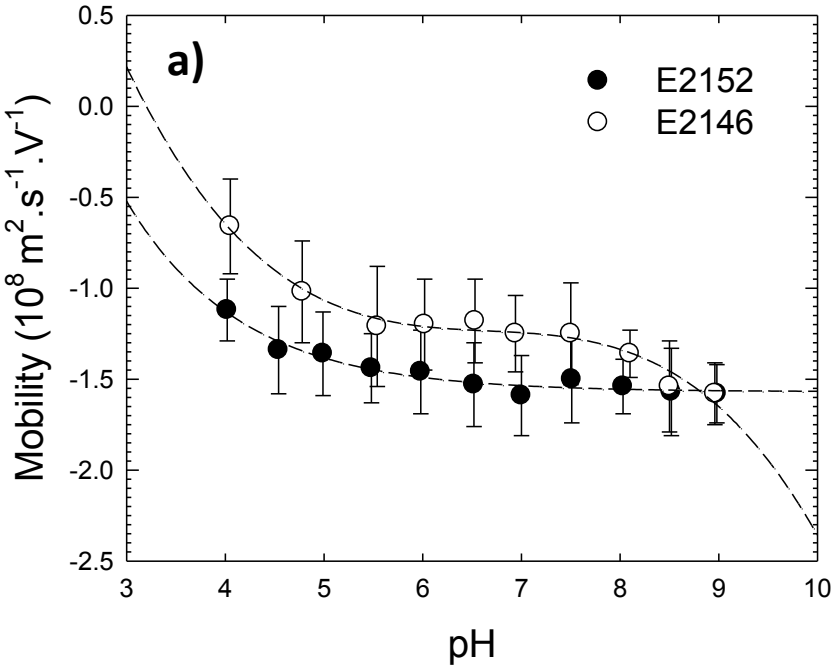
a)
E2152
E2146
Mobility (10^8 $m^2.s^{-1}.V^{-1}$)
pH

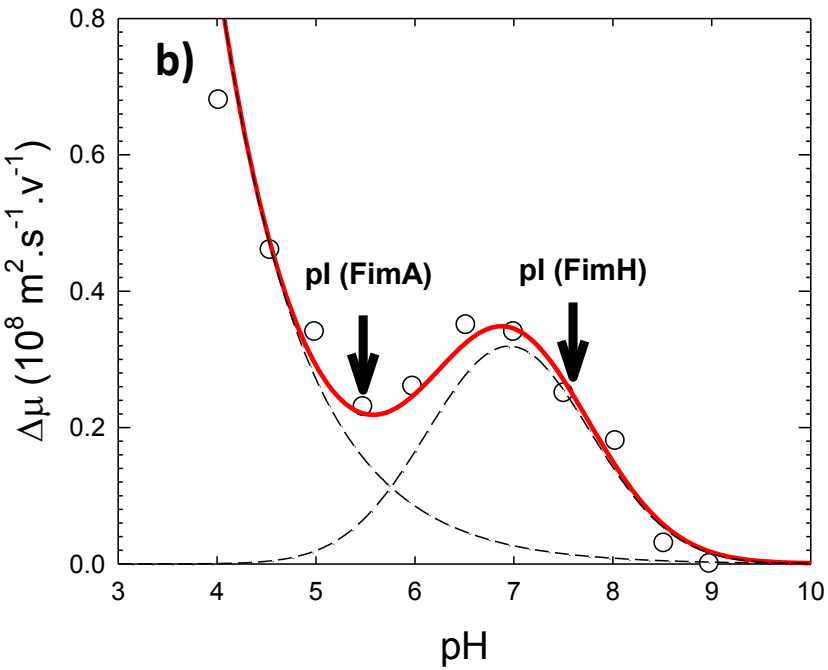
b)
pI (FimA)
pI (FimH)
Δμ (10^8 $m^2.s^{-1}.v^{-1}$)
pH

Figure 6.

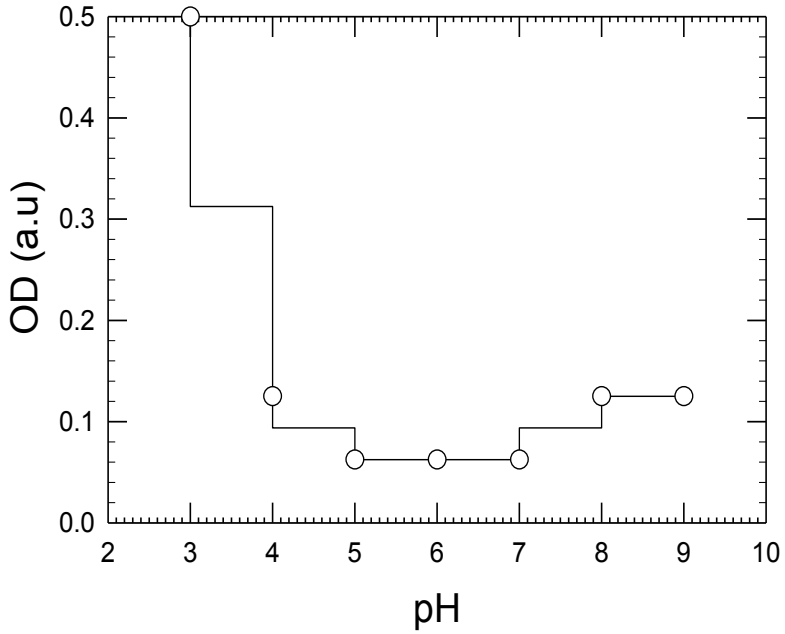

Figure 7.

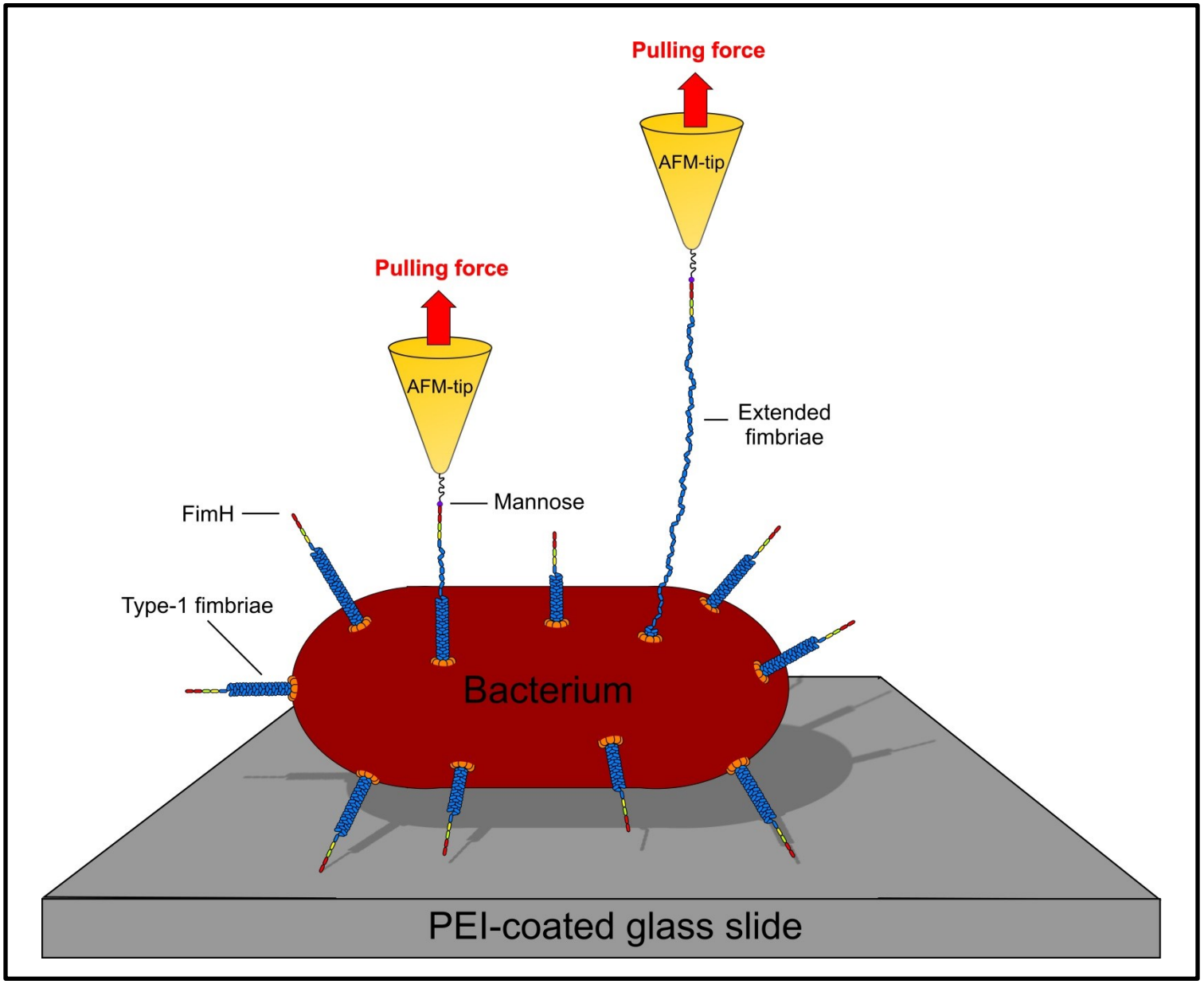
Pulling force
AFM-tip
Pulling force
AFM-tip
Extended fimbriae
Mannose
FimH
Type-1 fimbriae
Bacterium
PEI-coated glass slide

Figure S1.

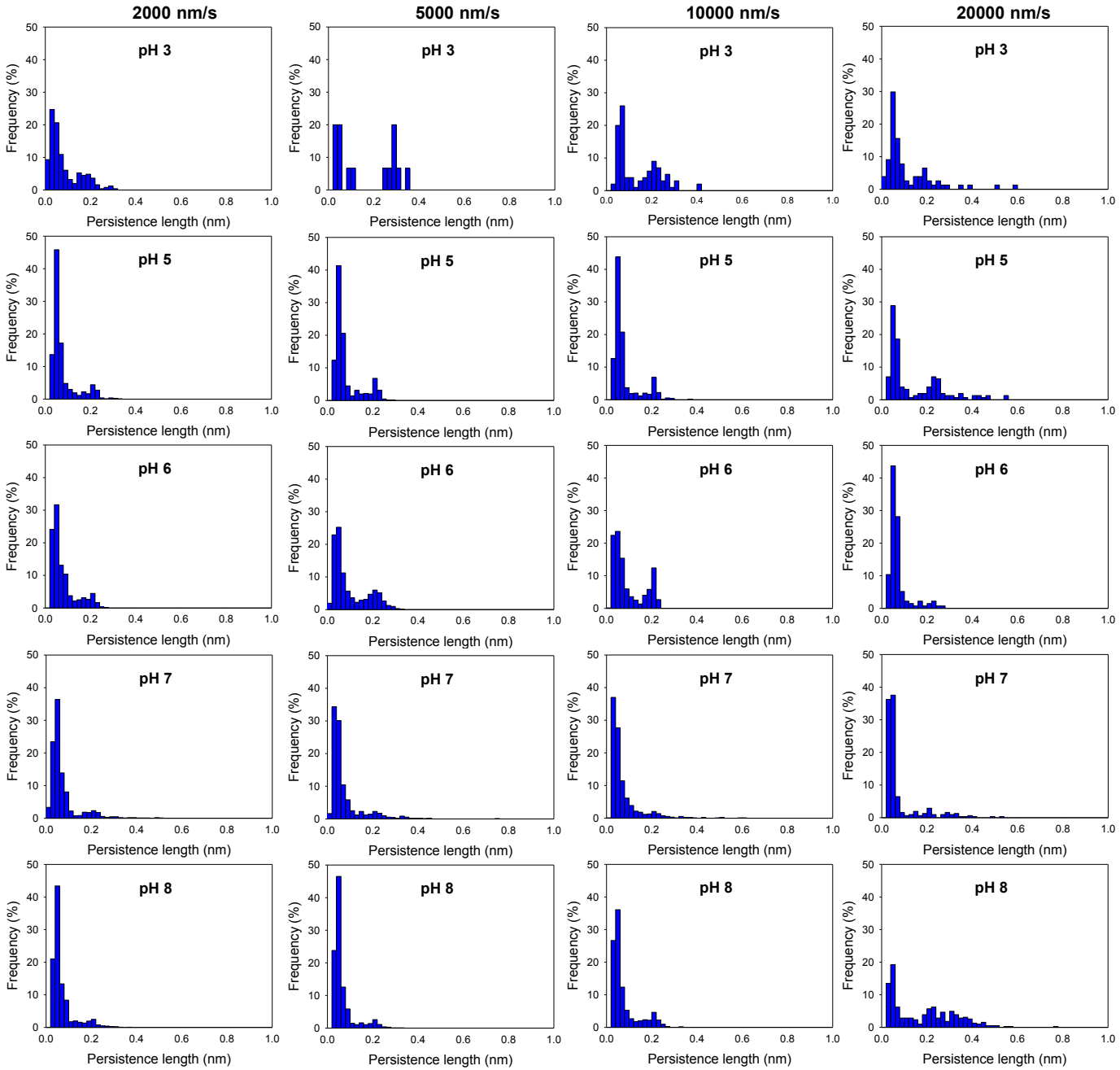
2000 nm/s
5000 nm/s
10000 nm/s
20000 nm/s
pH 3
pH 5
pH 6
pH 7
pH 8
Frequency (%)
Persistence length (nm)

Figure S2.

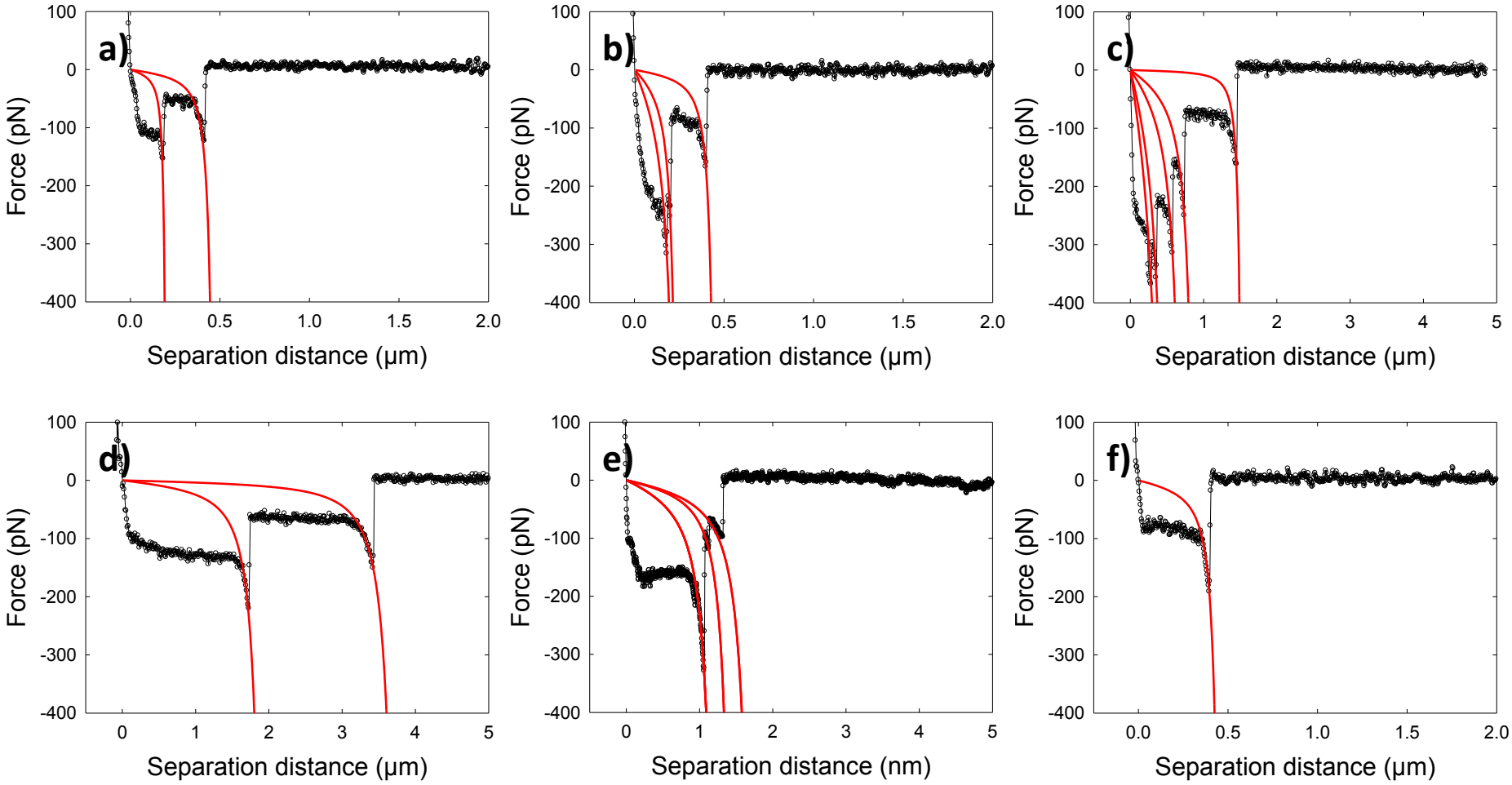
a)
b)
c)
d)
e)
f)
Force (pN)
100
0
-100
-200
-300
-400
0.0
0.5
1.0
1.5
2.0
0
1
2
3
4
5
Separation distance (μm)
Separation distance (nm)

Figure S3.

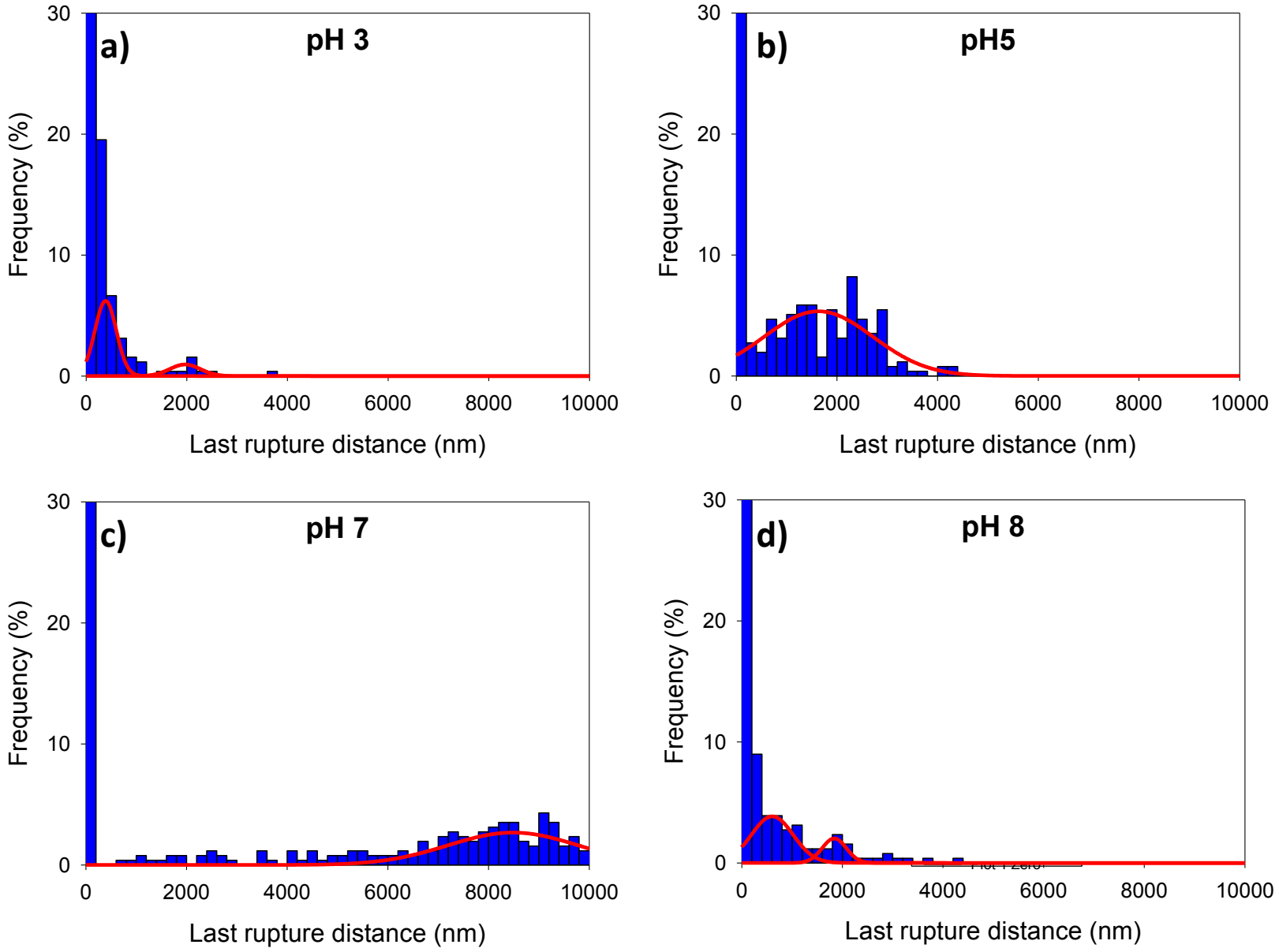
a)
pH 3
b)
pH5
c)
pH 7
d)
pH 8
Frequency (%)
Last rupture distance (nm)
0
10
20
30
0
2000
4000
6000
8000
10000

Figure S4.

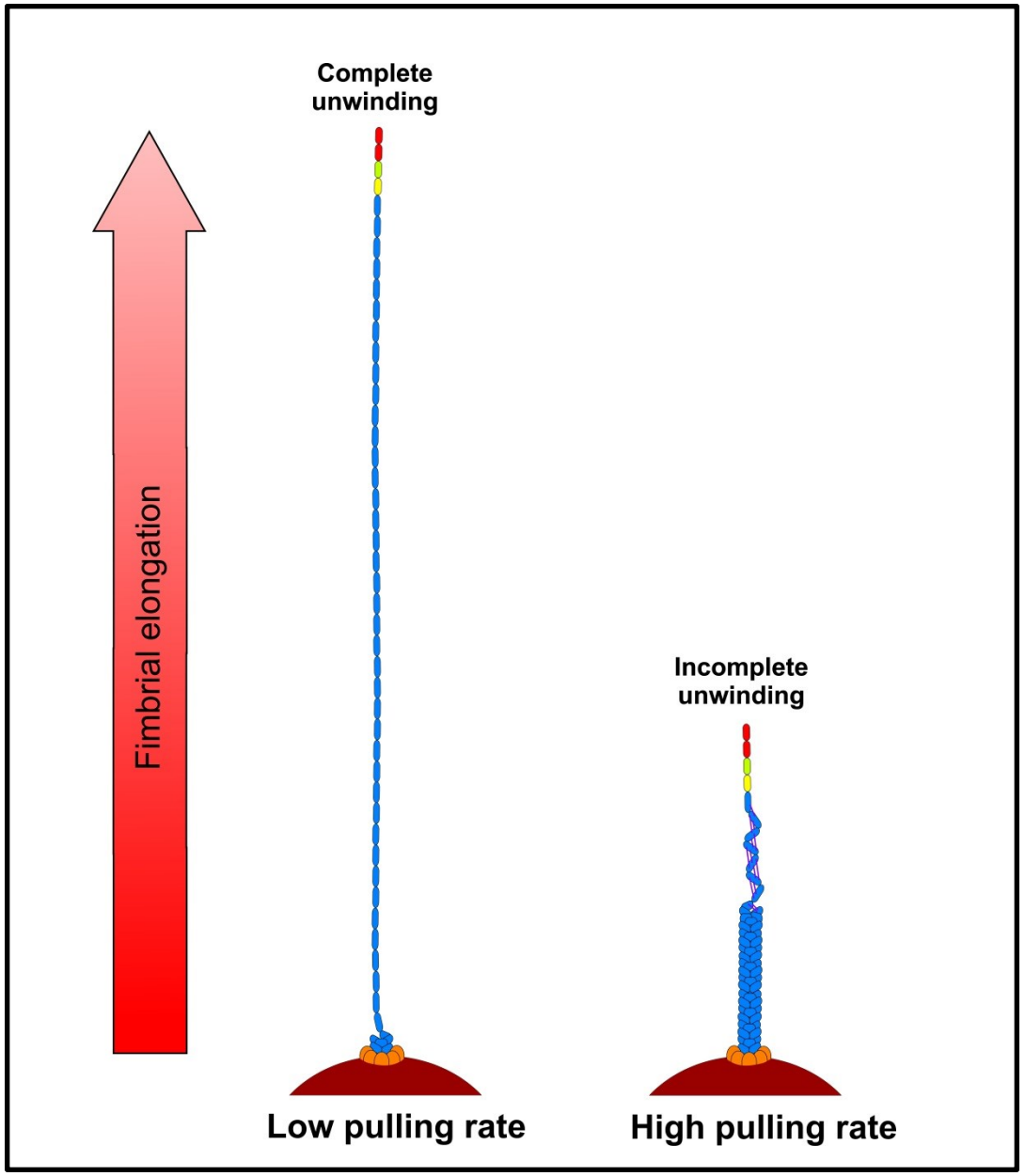
Complete
unwinding
Fimbrial elongation
Incomplete
unwinding
Low pulling rate
High pulling rate

Figure S5.

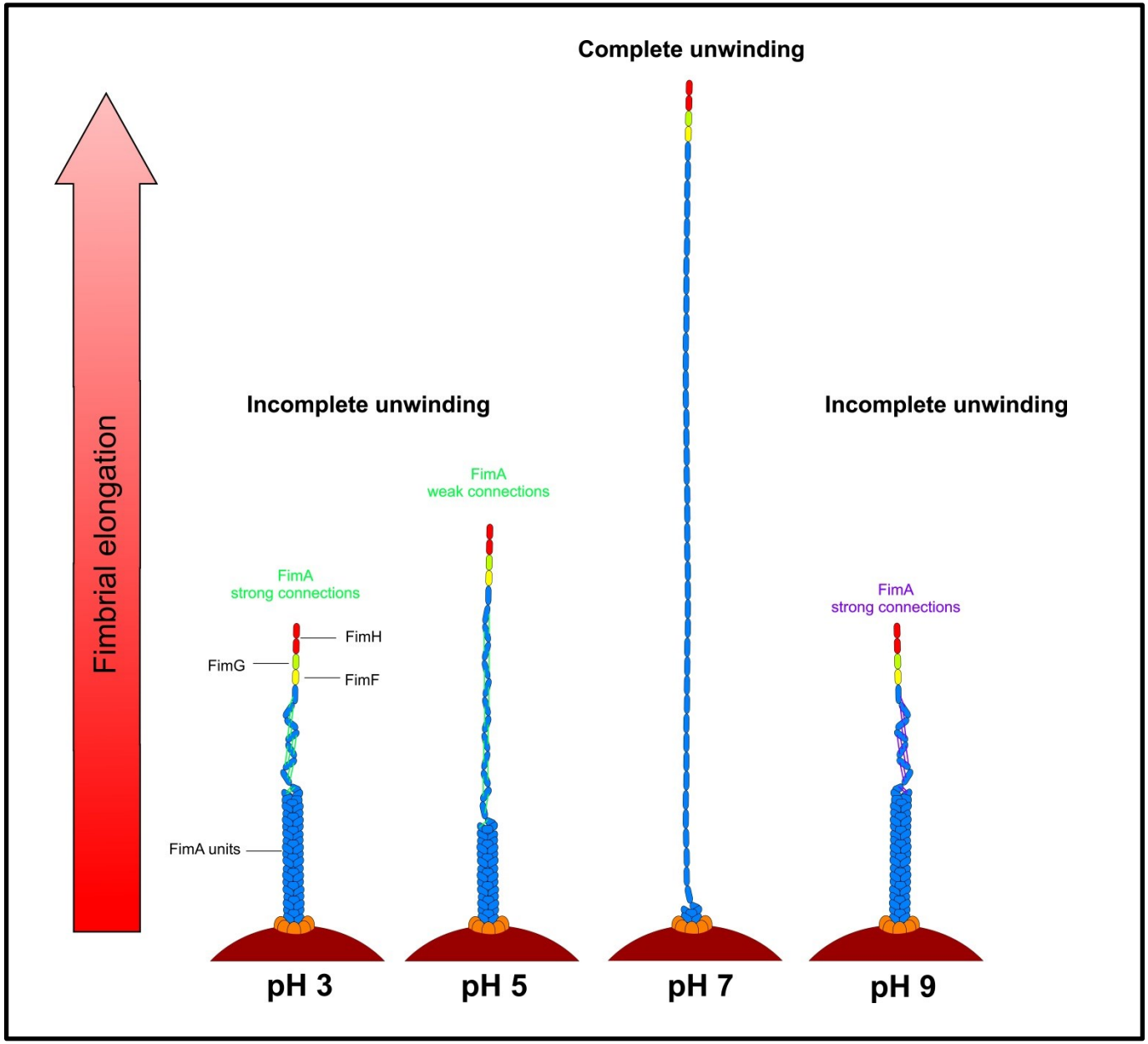
Complete unwinding
Fimbrial elongation
Incomplete unwinding
Incomplete unwinding
FimA
weak connections
FimA
strong connections
FimA
strong connections
FimH
FimG
FimF
FimA units
pH 3
pH 5
pH 7
pH 9

Figure S6.